iScience

Article

Sensory plasticity caused by up-down regulation encodes the information of short-term learning and memory

Graphical abstract

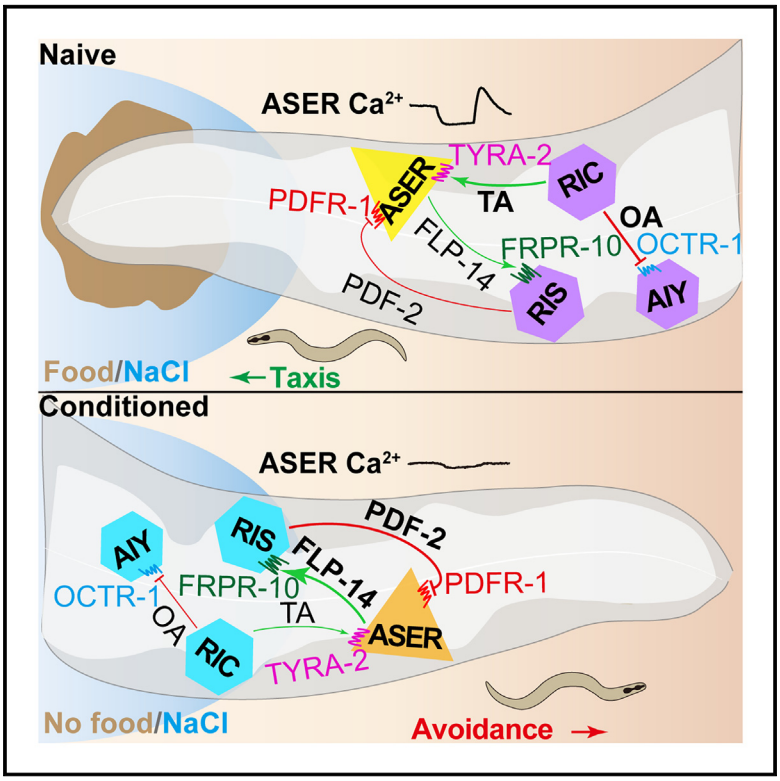

Highlights

- ASER sensory plasticity encodes the information of short-term salt chemotaxis learning
- RIC activity plasticity and ASER-RIS negative feedback cause ASER sensory plasticity
- Tyramine/TYRA-2 signaling engages in the sensory and behavioral plasticity
- FLP-14/FRPR-10 and PDF-2/PDFR-1 pathways mediate ASER-RIS negative feedback regulation

Authors

Ping-Zhou Wang, Ming-Hai Ge, Pan Su, ..., Li-Ming Chen, Tai-Hong Wu, Zheng-Xing Wu

Correspondence

taihongwu@hnu.edu.cn (T.-H.W.), ibbwuzx@mail.hust.edu.cn (Z.-X.W.)

In brief

Molecular biology; Neuroscience

Wang et al., 2025, iScience *28*, 112215
April 18, 2025
https://doi.org/10.1016/j.isci.2025.112215

CellPress

iScience

CellPress
OPEN ACCESS

Article

Sensory plasticity caused by up-down regulation encodes the information of short-term learning and memory

Ping-Zhou Wang,[1,3] Ming-Hai Ge,[1,3] Pan Su,[1,3] Piao-Ping Wu,[1] Lei Wang,[1] Wei Zhu,[1] Rong Li,[1] Hui Liu,[1] Jing-Jing Wu,[1] Yu Xu,[1] Jia-Lu Zhao,[1] Si-Jia Li,[1] Yan Wang,[1] Li-Ming Chen,[1] Tai-Hong Wu,[2,*] and Zheng-Xing Wu[1,4,*]

[1]Key Laboratory of Molecular Biophysics of Ministry of Education, Institute of Biophysics and Biochemistry, College of Life Science and Technology, Huazhong University of Science and Technology, Wuhan, China

[2]Hunan Research Center of the Basic Discipline for Cell Signaling, State Key Laboratory of Chemo and Biosensing, College of Biology, Hunan University, Changsha, China

[3]These authors contributed equally

[4]Lead contact

*Correspondence: taihongwu@hnu.edu.cn (T.-H.W.), ibbwuzx@mail.hust.edu.cn (Z.-X.W.)

https://doi.org/10.1016/j.isci.2025.112215

SUMMARY

Learning and memory are essential for animals' well-being and survival. The underlying mechanisms are a major task of neuroscience studies. In this study, we identified a circuit consisting of ASER, RIC, RIS, and AIY, is required for short-term salt chemotaxis learning (SCL) in *C. elegans*. ASER NaCl-sensation possesses are remodeled by salt/food-deprivation pared conditioning. RIC integrates the sensory information of NaCl and food availability. It excites ASER and inhibits AIY by tyramine/TYRA-2 and octopamine/OCTR-1 signaling pathways, respectively. By the salt conditioning, RIC NaCl calcium response to NaCl is depressed, thus, the RIC excitation of ASER and inhibition of AIY are suppressed. ASER excites RIS by FLP-14/FRPR-10 signaling. RIS inhibits ASER via PDF-2/PDFR-1 signaling in negative feedback. ASER sensory plasticity caused by RIC plasticity and RIS negative feedback are required for both learning and memory recall. Thus, the sensation plasticity encodes the information of the short-term SCL that facilitates animal adaptation to dynamic environments.

INTRODUCTION

Learning and memory (L&M) are essential for animals' well-being and survival in complex and dynamic environments. There are multiple forms of L&M. Different modules of L&M involve different neural structures and different mechanisms.[1] The neural structures or brain regions and circuits involved in learning memory activities may differ in different species of animals. However, the basic molecular, cellular, and circuital mechanisms of L&M are highly conserved in the animal kingdom.[2–4]

L&M being complex neural activities, involve sensation, neural signal transmission and its plasticity,[3,5,6] analytic integration of neural signals in neural circuits,[7,8] formation of new synapses or neural circuits, and changes in system-level activity.[9,10] For examples, habituation (the simplest form of implicit learning) involves activity-dependent presynaptic depression of synaptic transmission, sensitization and classical conditioning involve the presynaptic facilitation of synaptic transmission, long-term L&M involves the growth of new synaptic connections.[11–13] However, whether sensory plasticity functions in L&M remains an open issue.

The nematode *Caenorhabditis elegans* exhibits a great deal of behavioral plasticity and a broad range of learning and memory abilities in response to a variety of external stimuli, including that of mechanosensory, thermosensory, olfactory, gustatory, etc.[14–17] For this reason and because of its rapid life cycle, large number of progenies, ease of cultivation in a laboratory setting, a compact nervous system,[18] a better-worked-out toolbox of molecular genetics and neuronal manipulations, and a wide range of available behavior tests, *C. elegans* is a favored model system for investigating learning and memory.

Short-term salt chemotaxis learning (SCL) is a basic L&M model in *C. elegans*. *C. elegans* shows chemotaxis to sodium chloride (NaCl), a chemical as an indicant for the availability of bacteria food especially in laboratory conditions.[19] The direction and extent of the salt chemotaxis change depending on experience with salt and food. After the association of NaCl with a lack of food for a short period, *C. elegans* showed a dramatic reduction of chemotaxis to NaCl and eventually an avoidance of the salt (a negative chemotaxis against NaCl). This model of behavioral plasticity is termed as short-term salt chemotaxis learning or gustatory aversive learning.[17,20–22]

Multiple neurons, including ASER, AIB alone, and the combination of AIY and AIZ are needed for short-term SCL.[19] ASER senses NaCl stimulation and may function as site of the memory of the sensory experience.[23] Multiple classical neurotransmitters, neuromodulators, and neuropeptides are identified to engage in *C. elegans* SCL.[24] Among small molecule neurotransmitters and neuromodulators, tyramine (TA) and

octopamine (OA), function as important modulators for short-term SCL.[25,26] Several neuropeptides are known to function in *C. elegans* associative learning, including homologs of insulin (INS-1) and insulin-like peptides, oxytocin/vasopressin, myoinhibitory peptide (MIP-1/NLP-38), neuromedin U (CAPA-1/NLP-44), and elevenin (SNET-1).[27–35]

Neuropeptides function mainly by binding to G protein-coupled receptors (GPCRs). The *C. elegans* genome encodes an estimated 150 neuropeptidergic GPCRs.[36] Among them, many are orthologs of evolutionarily ancient receptors,[37,38] including orthologs of the oxytocin/vasopressin, gonadotropin-releasing hormone, thyrotropin-releasing hormone, neuromedin U, tachykinin, myoinhibitory peptide, and neuropeptide Y families.[27,32,33,37–39] Neuropeptidergic receptors offer a rich versatility for the regulation of physiological activities, including metabolism, growth and development, and behaviors in animal organisms, because of the diversity of receptors and signal transduction pathways.[40]

There are many neuropeptide-receptor interactions not yet identified in *C. elegans*. These interactions are challenges for their experimental characterization. Because many peptide-receptor interactions are promiscuous, weak, and transient in many cases, and considerably influenced by their context.[41] Many widely used structure determination methods, such as X-ray crystallography, may not be applicable to a great number of these interactions.[42] To save labor for studying peptide–receptor interactions, we use AlphaFold to predict potential peptide–receptor interactions related in this study. Most protein–protein interactions are determined by the 3D arrangement and the dynamics of interacting proteins. Recent successful efforts have been made to predict protein structure based on protein sequence, using deep neural network (artificial intelligence, AI) modeling methods, such as OmegaFold, ESMFold, and AlphaFold. The methods enable accurate modeling not only for protein monomer structures but also for protein complexes.[43–50] Therefore, using deep learning methods to predict neuropeptide-receptor interactions may provide a useful method for identifying neuropeptide-receptor interactions.

However, intensive studies have been made aiming to reveal molecular and circuital mechanisms underlying short-term SCL. However, pertinent questions remain unclear: what encodes the information of SCL? In this study, we used a reverse genetic screen, genetic manipulation, predictions of neuropeptide/receptor interactions by AlphaFold2, quantitative behavior assay, *in vivo* Ca^{2+} imaging, and neuronal manipulation to study the circuital mechanism underlying short-term SCL in *C. elegans*. We find that the ASER sensation of NaCl is suppressed during and after salt conditioning. ASER sensation remolding or sensory plasticity is caused by the top-down regulation from RIC and the negative feedback from RIS. It is required for both learning and memory recalling of short-term SCL and thus encodes the information of this L&M model. This finding suggests a mechanism for learning and memory.

RESULTS

Neuropeptidergic FLP-14/FRPR-10 signaling is required for salt chemotaxis learning

We used a modified test paradigm of salt chemotaxis learning developed by Wicks et al. in this study.[51,52] For mock and salt (food-deprivation/NaCl association) conditioning, about 200 animals of *C. elegans* were transferred into and immersed in food-free CTX solution without or with 100 mM NaCl for 20 min, respectively. Then, the animals were transferred onto a test agar plate to assay their chemotaxis to 20 mM NaCl (Figure 1A). The mock-conditioned wild-type (WT) N2 animal displayed strong chemotaxis to 20 mM NaCl (salt chemotaxis) indicated by chemotaxis index ($CI = (N_B - N_A)/(N_B + N_A)$). Here, N_A and N_B are the numbers of animals in the test regions without and with 20 mM NaCl, respectively. While the salt-conditioned WT N2 animal showed a negative salt chemotaxis or salt avoidance, that is the animal acquired salt chemotaxis learning (Figure 1B). We quantified salt chemotaxis learning (SCL) by learning index (LI), which was defined as: $CI_{mock} - CI_{conditioned}$. Here, CI_{mock} and $CI_{conditioned}$ are the chemotaxis index of mock-conditioned and salt-conditioned animals, respectively. To primarily examine whether neuropeptides engage in SCL, we used the loss-of-function (lof) mutant *egl-3*(*e1370*) animal. The gene *egl-3* encodes a proprotein convertase, EGL-3 that is required for the synthesis and processing of neuropeptide precursors.[53] The *egl-3* mutant displayed unchanged CI_{mock}, increased $CI_{conditioned}$, and reduced LI, in comparison with those in the WT N2 animal (Figures 1C and S1A), indicating that neuropeptides are involved in SCL.

The *C. elegans* genome encodes at least 153 neuropeptide-encoding genes that give rise to over 300 predicted bioactive peptides.[54,55] *C. elegans* neuropeptides fall into three families: insulin-like peptides,[56,57] FMRFamide (Phe-Met-Arg-Phe-NH2)-related peptides or FaRPs which are referred to as FLPs in *C. elegans*,[58] and neuropeptide-like proteins or NLPs.[40,59] We next used 19 *flp* and 13 *nlp* mutant animals to screen candidate neuropeptides engaging in SCL. Among the screened animals, the *flp-14*(*gk1055*) showed a severest defect in SCL, while all the mock-conditioned animals displayed WT CI_{mock} (Figures 1D and S1B–S1E). Therefore, we focused on *flp-14* in this study.

The *flp-14* gene encodes a propeptide that is processed to form four same peptide FLP-14.[60] (Figure S1F) The apparent learning deficiency observed in *flp-14*(*gk1055*) animal could arise from motor deficit, general defects in salt sensation, salt chemotaxis, and osmotic sensation. However, *flp-14*(*gk1055*) animal's locomotion speed and chemotaxis to NaCl of varied concentrations did not differ obviously from those of the WT N2 (Figures S1G and S1H). Moreover, the glycerol conditioning (association of food deprivation with 200 mM glycerol that osmotic pressure is equal to that of 100 mM NaCl for 20 min) did not affect salt chemotaxis in the *flp-14*(*gk1055*), contrarily to what was done by the salt conditioning (Figure S2A). These results support that the behavioral phenotype observed in the above experiment is an SCL defect and FLP-14 engages in SCL.

We next identified the candidate receptor of FLP-14. Known receptors of FLP-14 include FRPR-8, FRPR-19, NPR-1, NPR-4, NPR-6, NPR-11, NPR-39, NPR-40, DMSR-1, DMSR-3, and DMSR-7.[40,61–63] We thus used mutant and knocked-down animals of these receptors to examine their SCL phenotype. Among animals tested, only *npr-1*(*ad609*) animal displayed a learning defect that could not be restored to the WT by its genetic rescuing expression driven by the *npr-1* promoter, while all

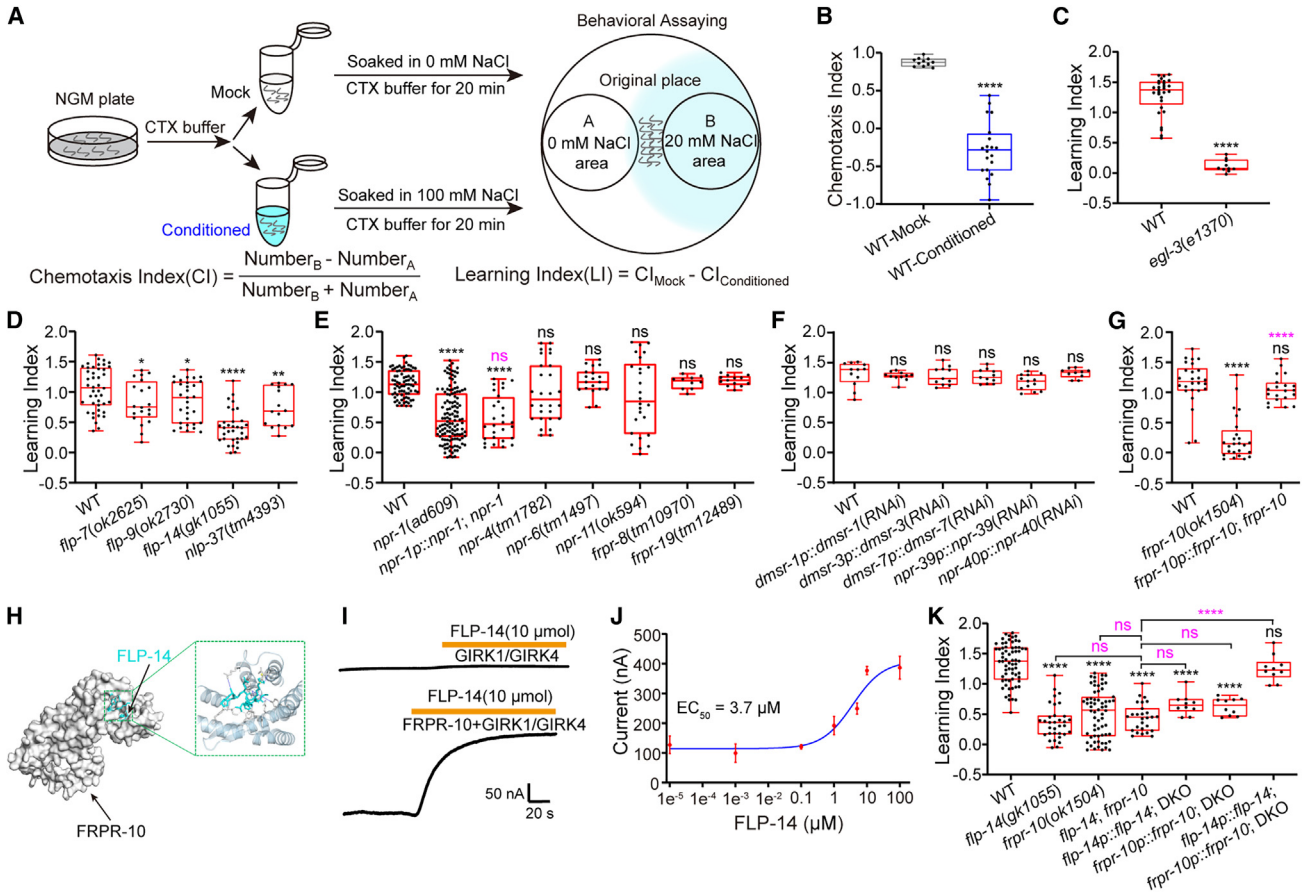

Figure 1. Neuropeptidergic FLP-14/FRPR-10 signaling is required for salt chemotaxis learning

(A) Diagram of the assay for salt chemotaxis learning used in this study. The inherent attraction of *C. elegans* animals to salt is dramatically decreased or turned into aversion after food-deprivation and 100 mM NaCl-CTX association conditioning for a short period of 20 min (Conditioned). In this behavioral test, mock-conditioned (Mock) animals, which were conditioned by the association of food-deprivation and CTX, are used as controls. The conditioned animals were assayed their chemotaxis to 20 mM NaCl on test agar plates containing test region without (region A) or with (region B) 20 mM NaCl in opposite direction. Chemotaxis index (CI) is calculated as: $(N_B - N_A)/(N_B + N_A)$. Here, N_A and N_B are the number of animals in the test regions A and B, respectively. The salt chemotaxis learning index (LI) in animals of a given genotype is calculated as $CI_{Mock} - CI_{Conditioned}$. Here, CI_{mock} and $CI_{conditioned}$ are the chemotaxis index in the mock-conditioned and salt-conditioned animals, respectively.

(B) Boxplots of chemotaxis index in the mock- (WT-Mock) and salt-conditioned (WT-Conditioned) wild-type (WT) N2 animals. Numbers of repeated tests: $n \geq 11$.

(C–G) Boxplots of learning indexes in the salt-conditioned WT N2 as a control, mutant, and transgenic animals, with each dot representing the data from each independent test. Numbers of repeated tests: $n \geq 10$.

(H) Illustration of neuropeptide FLP-14 (green) molecule bound in the putative binding-pocket of FRPR-10 receptor (gray).

(I) Representative current traces evoked by FLP-14 neuropeptides (10 μM) in the *X. laevis* oocyte injected with FRPR-10 cRNA.

(J) The dose response of the FLP-14-evoked currents with an EC_{50} of 3.7 μM fitted by the Hill equation.

(K) Boxplots of learning index in the salt-conditioned WT N2 as a control, mutant, and transgenic animals, with each dot representing the data from each independent test. Numbers of repeated tests: $n \geq 10$. The statistical significance of difference was analyzed by two-tailed *t* test with unpaired samples (B and C), or one-way analysis of variance with the post hoc test of Dunnett's correction (D, F) or Tukey's multiple comparison correction (E, G, K), and indicated as follows: ns, not significant, $^*p < 0.05$, $^{**}p < 0.01$, $^{****}p < 0.0001$, and in different colors for varied comparisons. Black, a comparison of the tested worms with the WT N2; magenta: a comparison of a gene-rescue transgenic animal vs. the related mutant or a comparison indicated.

animals showed WT CI_{mock} (Figures 1E, 1F, S2B, and S2C). This suggests that an unknown receptor or receptors mediate(s) FLP-14 action in SCL. For labor-saving, we employed AlphaFold 2 (AF2) to predict candidate FLP-14 receptor(s), by predicting interaction between FLP-14 and its candidate receptors. The 3D structure of a protein determines the function and interactions with other molecules. AF2 is powerful to accurately predict proteins' 3D structures from their amino acid sequences.[48] Thus, AF2 is useful in predicting ligand-receptor interaction.[44,50,64,65] Among examined receptor candidates, NPR-1, NPR-2, NPR-5, NPR-7, NPR-10, NPR-17, NPR-24, NPR-39, NPR-41, NPR-42, FRPR-1, FRPR-2, FRPR-4, FRPR-6, FRPR-7, FRPR-9, FRPR-10, FRPR-14, FRPR-15, and FRPR-17, have high scores ($\geq$4) of binding with FLP-14 (Table S1; Figure S2D). We assayed the SCL phenotype in the mutant or knocked-down animals of these receptors. The *frpr-10*(*ok1504*) and *npr-24*(*ok3192*) showed

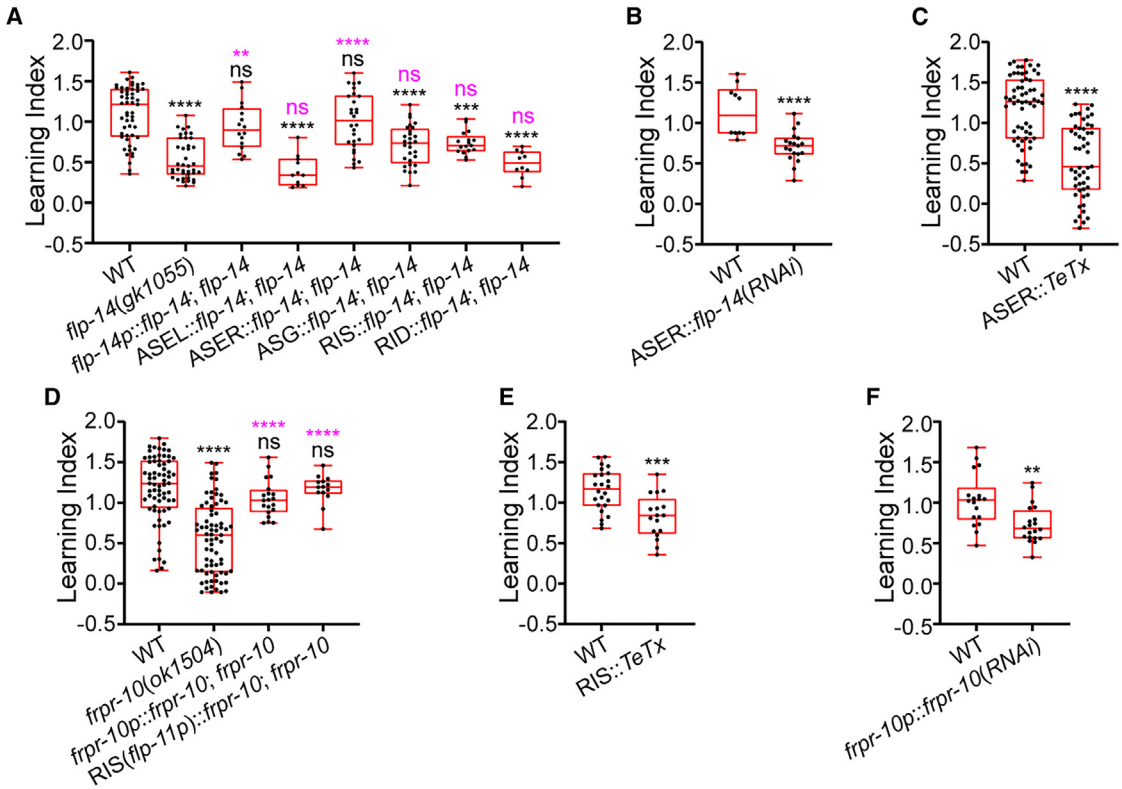

Figure 2. The FLP-14/FRPR-10 signaling required for salt chemotaxis learning may transmit neurotransmission from ASER to RIS

(A–F) Boxplots of learning index in the salt-conditioned wild-type N2 as a control, mutant, RNAi knocked-down, and transgenic animals, with each dot representing the data from each independent test. Numbers of repeated tests: $n \geq 10$. The statistical significance of difference was analyzed by one-way analysis of variance with the post hoc test of Tukey's multiple comparison correction (A, D) or two-tailed *t* test with unpaired samples (B, C, E, and F), and indicated as follows: ns, not significant, $^{**}p < 0.01$, $^{***}p < 0.001$, $^{****}p < 0.0001$, and in different colors for varied comparisons. Black: a comparison of tested worms with the WT N2; magenta, a comparison of a gene-rescue transgenic animal vs. the related mutant.

severe defects in SCL but maintained the WT chemotaxis to NaCl. The SCL phenotype in *frpr-10*(*ok1504*), but not in *npr-24*(*ok3192*), was restored to the WT by the genetic rescue. In addition, RNAi knockdown of *frpr-10* but not *npr-24* phenocopied genetic mutation (Figures 1G and S2E–S2H). The locomotion speed in *frpr-10*(*ok1504*) and salt chemotaxis in *frpr-10*(*ok1504*) and genetically rescued animals did not differ from those in the WT N2 animal (Figures S2I and S2J). AF2 modeling predicts that FLP-14 binds to the FRPR-10 putative-binding pocket in a tight conformation (Figure 1H). These indicate that the FRPR-10 receptor likely functions as a physiological receptor for FLP-14 in SCL.

FRPR-10 is a predicted G protein-coupled receptor.[66] We used a heterogeneous expression system to test the functional interaction between FRPR-10 and its ligand FLP-14, as previously reported.[67,68] Briefly, we injected 50 ng of FRPR-10 sense cRNA (complementary RNA) and 0.5 ng of GIRK (G protein-activated inwardly rectifying K^+)1 and GIRK4 sense cRNA into *Xenopus laevis* oocytes, and recorded whole-cell currents. Application of artificial peptide of FLP-14 generated a robust potassium current in FRPR-10/GIRK1/GIRK4 cells in a dose-dependent manner with a half maximal effective concentration (EC_{50}) of 3.7 μM, but no apparent current in GIRK1/GIRK4 cells (Figures 1I and 1J).

To further determine whether FLP-14 peptide functions through FRPR-10 in SCL *in vivo*, we constructed *flp-14* and *frpr-10* double knocked-out (*DKO*) animal and examined its SCL phenotype. The *DKO* animal displayed a defect in SCL but not in salt chemotaxis, similarly to the *flp-14*(*gk1055*) and *frpr-10*(*ok1504*) animals. The behavioral phenotype was restored to the WT only by the simultaneous rescue of both genes, but not by the single reconstitution of *flp-14* or *frpr-10* (Figures 1K and S2K). In conclusion, the above tests support that FRPR-10 is the receptor of FLP-14 and FLP-14/FRPR-10 signaling is required for SCL.

ASER-RIS circuit engages in salt chemotaxis learning

To pinpoint FLP-14's functional site(s) in the SCL circuit, we conducted fluorescent imaging, genetic analyses, and neuronal manipulation experiments. FLP-14 is expressed in main and secondary salt-sensitive gustatory ASE (Amphid Single Cilium E) and ASG (Amphid Single Cilium G) and interneuron RIS (Ring Interneuron S), identified by the expression pattern of GFP driven by a 2kb *flp-14* promoter (Figures S3A–S3E). The reconstitution of *flp-14* in its expression cells or ASER alone, but not in ASEL, ASG, or RIS, fully recovered the WT SCL behavior in the transgenic animal (Figures 2A and S3F), indicating *flp-14* functions

in ASER gustatory neuron. The neuron-specific *flp-14* knockdown by RNA interference (RNAi) reduced SCL ability in the salt-conditioned transgenic animal but had no obvious impact on salt chemotaxis in the mock-conditioned animal (Figures 2B and S3G). Moreover, ASER-specific neurotransmission elimination by TeTx, a light chain of tetanus toxin that is a specific protease of synaptobrevin[69] used to successfully inhibit chemical synaptic transmission in tested neurons (neuron:*TeTx* in short) in *C. elegans*,[70–76] not only suppressed SCL but also salt chemotaxis (Figures 2C and S3H). These results support that FLP-14 functions in ASER.

We analyzed FRPR-10's functional site(s) in the SCL circuit, using a similar strategy used in the study of FLP-14. FRPR-10 is expressed in single interneuron RIS, identified by the expression pattern of GFP driven by *frpr-10* promoters with a varied length of 1 kb, 2 kb, and 4 kb (Figures S3I–S3L). The *frpr-10* reconstitution in RIS driven by promoters of *frpr-10* (2 kb) and *flp-11* (2 kb) fully rescued SCL defect (Figures 2D and S3M). Moreover, the RIS::*TeTx* neuronal inhibition and RIS-specific *frpr-10* knockdown by RNAi, but not *RFP* knockdown (for examining RNAi potential impact on cell's physiology of RNAi transcripts), significantly reduced the learning ability (Figures 2E, 2F, S3N, S3O, S3P, and S3Q). These support that FLP-14/FRPR-10 signaling mediates neurotransmission from ASER to RIS and engages in SCL.

What is the effect of FLP-14/FRPR-10 signaling on RIS activity and its underlying mechanism? To answer this issue, we measured RIS Ca^{2+} signals in response to 50 mM NaCl stimulation after the salt conditioning. No obvious change in Ca^{2+}-responses in RIS was observed (Figures S4A and S4B). FRPR-10 receptor is a predicted G protein-coupled receptor.[66] It is possible that FRPR-10 signaling does not affect RIS excitability indicated by Ca^{2+} signals but regulates neurotransmitter and/or neuropeptide release by the activation of G proteins. G proteins are usually extensively expressed in various tissues or cells. We thus used RIS-specific RNAi knockdown of pan-neuronally expressed genes encoding α-subunit of heterotrimeric G proteins, *gsa-1* (G_s), *egl-30* (G_q), and *goa-1* (G_i),[77] to preliminarily identify potential signaling pathway(s). The RIS-specific RNAi knockdown of *gsa-1* and its effect gene *acy-1* (encoding adenylate cyclase-1, ACY-1), but not *egl-30* or *goa-1*, decreased LI or suppressed SCL (Figures S4C and S4D). This suggests that FRPR-10 functions through the Gs-ACY-1 signaling pathway (Figure S4E). Taken together, the ASER-RIS circuit engages salt chemotaxis learning.

The FLP-14/FRPR-10 signal pathway in RIS mediates ASER sensory plasticity in the salt chemotaxis learning process

Since ASEs are the main salt sensory neurons and FLP-14 neuropeptide released by ASER is involved in SCL. We thus examined ASE sensory responses to NaCl after mock and salt conditioning, using Ca^{2+} fluorescence imaging. ASER Ca^{2+} signals in response to the stimulation of 20 mM and 50 mM NaCl in the mock-conditioned WT N2 animal displayed a robust hyperpolarization (inhibitory) ON response and an even stronger depolarization (excitatory) OFF-response. Interestingly, the ASER Ca^{2+} signals of both ON- and OFF-responses in the salt-conditioned animal were nearly disappeared. The intensities of ON- and OFF-responses to 50 mM NaCl were stronger than those to 20 mM NaCl (Figures 3A–3C and S4F–S4H). Thus, we used 50 mM NaCl in this study. This result indicates that ASER salt sensation is remolded in the SCL process. We then introduced the sensory plasticity index to indicate the ASER sensation change. The sensory plasticity index of ON- and OFF-responses to 50 mM NaCl stimulation in the salt-conditioned WT N2 animal were similar (around 0.8) and bigger than those of responses to 20 mM NaCl stimulation (Figures 3D and S4I). Does ASEL activity change after the salt conditioning such as ASER? ASEL only displayed a robust ON-response but no obvious OFF-response to 50 mM NaCl stimulation in the mock- and salt-conditioned WT N2 animals. Moreover, the ASEL Ca^{2+}-response in the salt-conditioned animal almost copied that in the mock-conditioned animal. (Figures 3E–3G). These indicate that ASEL salt sensation is not modulated in the SCL.

Given that FRPR-10 signaling in RIS is essential for SCL, a logical issue is that this signaling very likely mediates sensory plasticity in ASER. Expectedly, ASER sensory plasticity in the salt-conditioned *frpr-10*(*ok1504*) animal was dramatically reduced and fully restored to the WT by *frpr-10* reconstitution in RIS (Figures 3H–3J). Moreover, ASER sensory plasticity in the salt-conditioned *flp-14*(*gk1055*) and ASER-specific *flp-14*-rescued animals almost phenocopied that in the *frpr-10* mutant and RIS-specific *frpr-10* rescued animals (Figures 3K–3M).

Based on the above results, we conclude that FLP-14/FRPR-10 signaling is not only required for SCL but also for ASER plasticity and that sensory plasticity may be a mechanism of the short-term learning and memory.

Neuropeptide PDF-2 released from RIS up-regulates salt chemotaxis learning and ASER sensory plasticity

Given that FRPR-10 signaling in RIS is required for both SCL and ASER plasticity, RIS should regulate ASER sensory plasticity in the process of SCL. What is the mechanism for RIS regulating SCL and ASER sensory plasticity? Single interneuron RIS is GABAergic and neuropeptidergic.[78,79] It is chemically or electrically connected with locomotion-regulating neurons, such as AIB (Anterior Interneuron B) (electrically), AVE (Anterior Ventral Process E), RIM (Ring Interneuron M), SMD (Sublateral Motor Neuron D), and motor neurons DB (Dorsal B-type Motor Neuron). However, there is no known synaptic connection between RIS and ASE.[18,80] Thus, RIS may modulate ASER activity by neurohumoral regulation. For analyzing RIS function in SCL, we used RIS-specific RNAi knockdown of *unc-25* (encodes a glutamic acid decarboxylase the essential for GABA biosynthesis), *egl-3* (encodes a proprotein convertase), *inx-6*, *inx-7*, and *unc-9* (encode *C. elegans* gap-junction proteins, expressed in RIS),[53,78,81,82] to test SCL behavior in the transgenic animals. All transgenic animals showed reduced learning index and the WT CI_{mock} (Figures S5A and S5B). This indicates that chemical and electrical synapse connections and neuropeptide(s) from RIS are required for SCL. For detecting RIS regulatory role in ASER sensory plasticity, we used lof mutant animals of *unc-25*, *egl-3*, and *unc-9* to assay ASER Ca^{2+}-responses to 50 mM NaCl stimulation after mock and salt conditioning and to analyze ASER sensory plasticity. As shown in Figures S5C–S5K, the

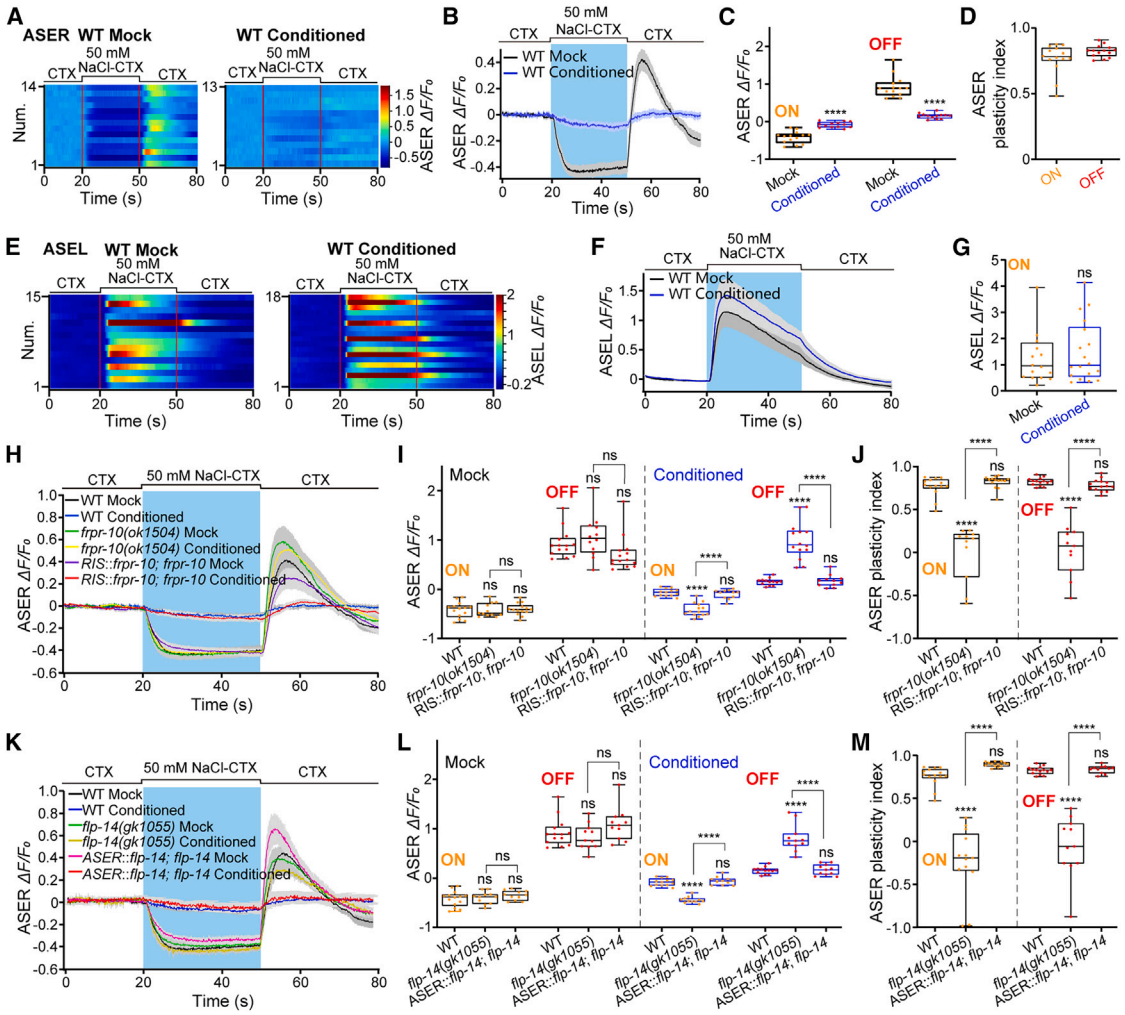

Figure 3. FLP-14/FRPR-10 signaling engages in ASER sensory plasticity

(A) Heat maps of the relative changes in calcium (Ca^{2+}) transients in the soma of ASER sensory neurons in the mock- (Mock) and salt-conditioned (Conditioned) wild type (WT) N2 worms. Red lines mark the time of the switch between CTX buffer and 50 mM NaCl-CTX solution. $\Delta F = F - F_0$. F is the average fluorescence intensity of the region of interest of neuronal soma in each frame; F_0 is the average intensity within 20 s before the stimulation. The average background signal from all frames was subtracted from F and F_0. The label on the left y axis indicates the tested animals' number (Num.). Numbers of tested animals: $n \geq 13$. The same hereinafter.

(B) Curves of ASER Ca^{2+}-responses in response to 50 mM NaCl stimulation in the mock- and salt-conditioned WT N2 animals. The Ca^{2+} signals were measured using the R-GECO1.0 as a Ca^{2+} indicator. Ca^{2+} transients were presented as curves of means (solid traces) ± SEM (gray shading), with light-cyan background indicating the application of 50 mM NaCl/CTX solution. The same hereinafter.

(C) Boxplots of the average intensity of Ca^{2+} signals in the plateau phase (30 s–50 s) of ON response and amplitude of the OFF-response in ASER. The amplitude of the OFF-response is defined as the peak amplitude of OFF-response minus the average value of ON-response. Each yellow or red dot represents the data of ON- or OFF-responses in each tested animal.

(D) Boxplots of ASER plasticity index in the salt-conditioned WT N2 animals. The plasticity index is calculated as: $(ON_{mock} - ON_{conditioned})/ON_{mock}$ and $(OFF_{mock} - OFF_{conditioned})/OFF_{mock}$.

(E) Heat maps of relative changes in Ca^{2+} signals in the soma of ASEL sensory neurons in the mock- (Mock) and salt-conditioned (Conditioned) WT N2 worms. Numbers of tested animals: $n \geq 15$.

(F) Curves of NaCl-induced Ca^{2+} responses in ASEL neurons in the indicated animals in the mock- and salt-conditioned WT N2 animals.

(G) Boxplots of the averaged intensity of Ca^{2+} signals in the plateau phase (20 s–50 s) and peak amplitude of ON response in ASEL.

(H–J) Curves and boxplots of ASER Ca^{2+} responses and plasticity index in the indicated animals, respectively. Numbers of tested animals: $n \geq 11$.

(K–M) Curves and boxplots of ASER Ca^{2+} responses and plasticity index in the indicated animals, respectively. Numbers of tested animals: $n \geq 11$. The statistical significance of difference was analyzed by two-tailed t test with unpaired samples (C, D and G) or one-way analysis of variance with the post hoc test of Tukey's multiple comparison correction (I, J, L and M), and indicated as follows: ns, not significant, ****$p < 0.0001$, in comparison with the control WT N2.

egl-3(*gk238*) but not *unc-25*(*ok1901*) or *unc-9*(*fc16*), displayed significant changes in ON- and OFF-responses to the salt stimulation and defect of sensory plasticity after salt conditioning but not mock conditioning, in comparison with those of the WT N2. The above results suggest that synaptic neurotransmission from RIS is required only for SCL but not for ASER sensory plasticity, while RIS neurohumoral regulation is essential for both SCL and ASER sensory plasticity.

RIS expresses neuropeptide-encoding genes pigment dispersing factor 2, *pdf-2*, also named *nlp-37*.[79] The *nlp-37*(*tm4393*) animal displayed a significant defect of SCL, and exhibited the WT CI_{mock} (Figures S1B and S1C), suggesting PDF-2 or NLP-37 may mediate SCL. PDF-2 receptor PDFR-1 is expressed in muscle cells and multiple neurons including ASER.[83] We thus used genetic analyses of *pdf-2* and *pdfr-1* to detect the roles of these two genes in SCL and ASER sensory plasticity. As expected, lof mutation of *pdf-2* reduced the SCL index that was restored to the WT by genetic rescue driven by both *pdf-2p* and RIS-specific promoters (Figures 4A and S5L). Although lof mutation of *pdfr-1* decreased SCL ability that rescued to the WT by genetic reconstitution driven *pdfr-1p*. However, the *pdfr-1* reconstitution in ASER alone could partially rescue the behavioral defect (Figures 4B and S5M). *pdfr-1* is expressed extensively in muscle cells and neurons, including sensory neurons, interneurons, and motor neurons. The *pdfr-1* mutant animal showed a defect in locomotion.[84] Thus, we examined the SCL, chemotaxis, and locomotion phenotypes in the ASER-specific *pdfr-1* RNAi knocked-down animal. The *pdfr-1* knockdown impaired SCL such as the RIS-specific knockdown of *pdf-2* but did not affect chemotaxis and locomotion speed (Figures 4C, S5N, and S5O). These results suggest that PDF-2/PDFR-1 signaling acts on ASER to regulate SCL behavior.

PDF-2/PDFR-1 signaling should regulate or control ASER sensory plasticity. We used animals of *pdf-2* and *pdfr-1* mutation and transgenic rescue to detect ASER Ca^{2+}-responses to 50 mM NaCl stimulation and analyze sensory plasticity after mock- and salt-conditioning. Expectedly, ASER in the salt-conditioned *pdf-2* or *pdfr-1* animals showed robust ON- and OFF-responses to the salt stimulation which were almost eliminated by the genetic reconstitution of *pdf-2* in RIS or *pdfr-1* in ASER. In other words, ASER sensory plasticity in the salt-conditioned mutant animals were almost disappeared and was restored to the WT by the genetic rescue of *pdf-2* in RIS or *pdfr-1* in ASER (Figures 4D–4I). In summary, the PDF-2/PDFR-1 signaling pathway mediates the neurohumoral regulation of ASER by RIS in the top-down regulation of SCL and ASER sensory plasticity.

RIC excites and inhibits ASER and AIY in the regulation of salt chemotaxis learning by tyraminergic TYRA-2 and octopaminergic OCTR-1 signaling

Food deprivation is a conditioning stimulation for SCL.[19] Paired RIM and mainly RIC interneurons service as a center for integrating the sensory information of stress and starvation or food deprivation.[73,85–91] RIM and RIC release TA and OA, respectively. Octopamine released from RIC leads to the activation of the transcription factor CREB required for long-term learning and memory.[92,93] TA is synthesized from tyrosine catalyzed by tyrosine decarboxylase TDC-1. OA is transformed from TA catalyzed by tyramine-beta-hydroxylase TBH-1. The genes *tdc-1* and *tbh-1* encode TDC-1 and TBH-1 respectively. *tdc-1* is expressed in RIM and RIC, while *tbh-1* is mainly expressed in RIC.[94] Thus, we used *tdc-1* and *tbh-1* mutant animals to test their SCL phenotype. Expectedly, SCL ability was reduced in the *tbh-1* and *tdc-1* mutant animals without change in CI_{mock}. The behavioral defects in the mutant animals were eliminated by the genetic reconstitution of each gene driven by each promoter. However, the *tdc-1* reconstitution in RIC but not in RIM eliminated the behavioral defect caused by the *tdc-1* mutation (Figures 5A and S6A). This suggests RIC but not RIM engages in SCL. We next used pharmacological test in the *tdc-1*; *tbh-1* double knockout (*DKO*) animal to identify the function of TA and OA or RIC and RIM neurons in SCL. Administration of TA, OA, or both had no obvious impact on SCL and salt chemotaxis in the WT N2 animal. Puzzlingly, neither the treatment of OA nor that of TA, but the application of both OA and TA restored the WT SCL in the *DKO* animal (Figures 5B and S6B). Possibly, RIC releases both TA and OA and has more than one function site. We then used neurotransmission inhibition by RIM::*TeTx*, RIC::*TeTx*, and RIM/RIC::*TeTx* to validate the above results. RIC::*TeTx* and RIC/RIM::*TeTx* similarly suppressed SCL, while RIM::*TeTx* had no obvious impact on the behavior (Figures 5C and S6C). In summary, these tests indicate that RIC but not RIM engages in SCL, and RIC possibly has multiple function effect cells through both TA and OA signal pathways.

Does RIC activity change after salt/food deprivation conditioning? To answer this issue, we performed RIC Ca^{2+}-imaging with G-CaMP3.0 as an indicator. RIC displayed a minor excitatory ON-response of Ca^{2+} transients in the mock-conditioned WT N2 animals. After salt/food-deprivation association conditioning, the RIC Ca^{2+}-response almost disappeared and significantly differed from that in the mock-conditioned animal (Figures 5D and 5E). This suggests that RIC activity in response to the NaCl stimulation is inhibited after the salt conditioning and support RIC engages in SCL.

What are TA and OA receptors functioning in SCL? Among mutant animals of known TA receptors TYRA-2, TYRA-3, SER-2, LGC-55, and OA receptors OCTR-1, SER-3, and SER-6, the *tyra-2*(*tm1846*), *tyra-2*(*tm1815*), and *octr-1*(*ok371*) displayed obvious behavioral defect, while all animals showed the WT CI_{mock} (Figures S6D–S6G). SCL defect caused by *tyra-2* and *octr-1* lof mutation was removed by the genetic reconstitution of each gene driven by its promoter. We thus used the genetic reconstitution of these two genes to identify their functional sites. Our test result showed that among multiple neuron(s)-specific constitution of *tyra-2* or *octr-1*, rescue expression of *tyra-2* in ASER (driven by 3.2 kb *gcy-5p*) and *octr-1* in AIY (directed by 4.0 kb *T19C4.5p*) fully restored the WT SCL in the transgenic animals (Figures 5F, 5G, S6H, and S6I). We then used neurotransmission inhibition by AIY::*TeTx* to validate whether AIY functions in SCL and found AIY::*TeTx* impaired SCL (Figures S6J and S6K). These results support that tyraminergic TYRA-2 and octopaminergic OCTR-1 signaling pathways act in ASER and AIY to generate SCL behavior. To assay AIY Ca^{2+} responses to the NaCl stimulation in mock- and salt-conditioned animals, we performed Ca^{2+}-imaging with G-CaMP3.0 as an indicator. AIY displayed only a minor inhibitory and excitatory

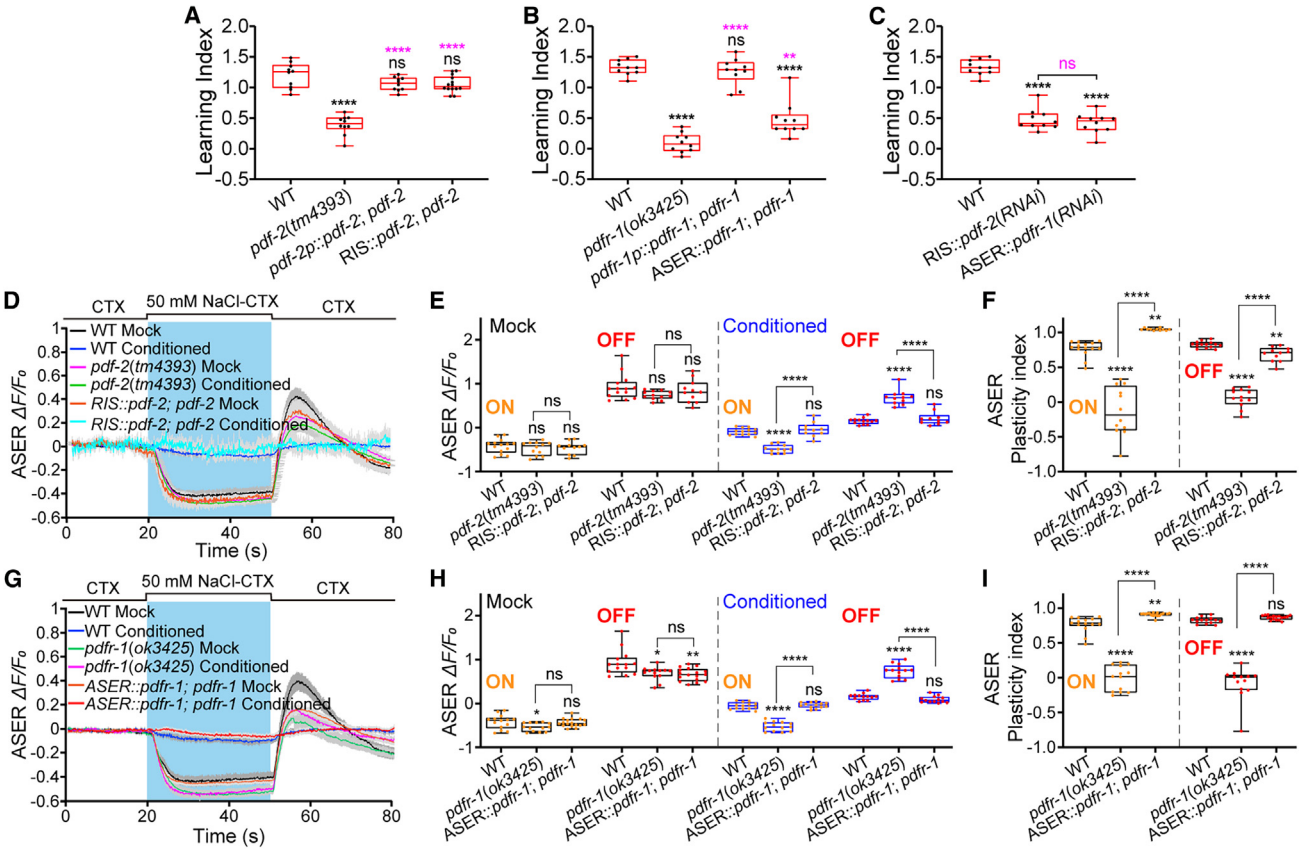

Figure 4. PDF-2/PDFR-1 signaling pathway prompts salt chemotaxis learning

(A–C) Boxplots of learning index in the salt-conditioned wild type (WT) N2, mutant, and transgenic animals, with each dot representing the data from each independent test. Numbers of repeated tests: $n \geq 10$.

(D) Curves of NaCl-induced calcium responses in ASER neuron in the mock- and salt-conditioned WT N2, *pdf-2*(*tm4393*) and RIS:*pdf-2* transgenic animals. Ca^{2+} signals were measured using the R-GECO1.0 as a Ca^{2+} indicator. Ca^{2+} transients were presented as curves of means (solid traces) ± SEM (gray shading).

(E) Boxplots of the average intensity of Ca^{2+} signals in the plateau phase (30 s–50 s) of ON response and amplitude of the OFF response in ASER. The amplitude of the OFF response is defined as the peak amplitude of the OFF response minus the average value of the ON response. Each yellow or red dot represents the data of ON- or OFF-responses in each tested animal. Numbers of tested animals: $n \geq 10$.

(F) Boxplots of ASER plasticity index in the salt-conditioned WT N2, *pdf-2*(*tm4393*), and RIS:*pdf-2* transgenic animals. The plasticity index was calculated as: $(ON_{mock} - ON_{conditioned})/ON_{mock}$ and $(OFF_{mock} - OFF_{conditioned})/OFF_{mock}$.

(G–I) Curves and boxplots of ASER Ca^{2+} responses and plasticity index in the indicated animals. Numbers of tested animals: $n \geq 13$. The statistical significance of difference was analyzed by one-way analysis of variance with the post hoc test of Tukey's multiple (A–C, E, F, H, and I) and indicated as follows: ns, not significant, $^{*}p < 0.05$, $^{**}p < 0.01$, and $^{****}p < 0.0001$, and in different colors for varied comparisons. Black: a comparison of tested worms with the WT N2; magenta, a comparison of a gene-rescue transgenic animal vs. the related mutant or as indicated.

ON-response of Ca^{2+} transients in the mock- and salt-conditioned WT N2 animals, respectively (Figures S6L and S6M). Combined with the suppressed RIC Ca^{2+}-response to NaCl stimulation in salt-conditioned animals, this suggests that RIC may inhibit AIY activity by OA/OCTR-1 signaling. RIC suppression by salt-conditioning removes its inhibition on AIY and thus alters chemotaxis to NaCl.

ASER and RIS form a negative feedback circuit essential for SCL, in which ASER possibly activates RIS to release neuropeptide PDF-2 through FLP-14/FRPR-10 signaling, and RIS inhibits ASER activity via PDF-2/PDFR-1 signaling (Figures 2 and 3). RIC functions in SCL through TYRA-2 and OCTR-1 act in ASER and AIY, respectively (above result). Thus, RIC, ASER, and RIS may form a functional circuit to regulate SCL behavior. To answer this issue, we analyzed the functions of TYRA-2 and FRPR-10 signaling pathways acting in ASER in SCL using genetic analyses of *tyra-2* and *frpr-10*. The double knockout of *tyra-2* and *frpr-10* impaired SCL like that of single knockout of *tyra-2* or *frpr-10*. The SCL phenotype was restored to the WT only by the genetic reconstitution of both *tyra-2* and *frpr-10*, not by that of a single gene of *tyra-2* or *frpr-10* (Figures 5H and S6N). This supports the idea that RIC, ASER, and RIS form a circuit to modulate the short-term SCL behavior.

ASER sensory plasticity encodes the information of the short-term salt chemotaxis learning

TYRA-2 signaling functions in SCL; it should act on ASER sensory plasticity. We thus employed genetic analyses of *tdc-1*

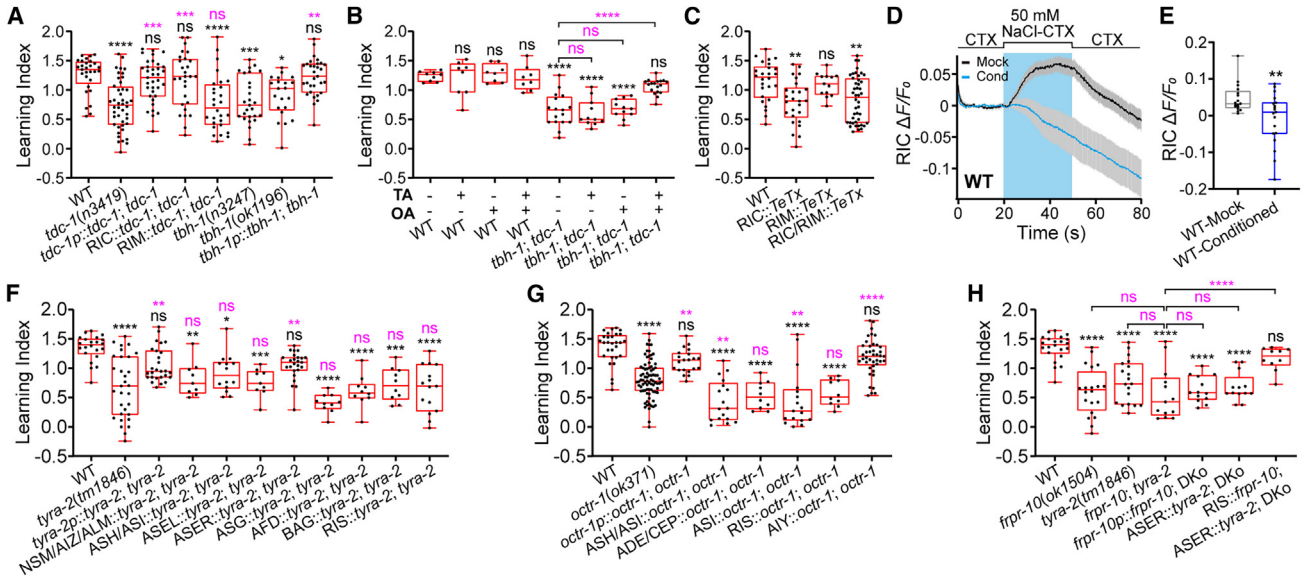

Figure 5. RIC drives salt chemotaxis learning via the signaling of tyraminergic TYRA-2 in ASER and octopaminergic OCTR-1 in AIY

(A–C) Boxplots of learning index in the salt-conditioned wild-type (WT) N2 as a control, mutant, and transgenic animals, with each dot representing the data from each independent test. Numbers of repeated tests: $n \geq 8$.

(D) Curves of NaCl-induced calcium (Ca^{2+}) responses in RIC neuron in the mock- and salt-conditioned WT N2 animal. The Ca^{2+} signals were measured using the G-CaMP3.0 as a Ca^{2+} indicator and presented as curves of means (solid traces) ± SEM (gray shading), with light-cyan background indicating the application of 50 mM NaCl/CTX solution.

(E) Boxplots of the average intensity of Ca^{2+} signals of RIC during stimulation (20 s–50 s) with each dot representing the data from each tested worm's ON response. Numbers of tested animals: $n \geq 17$.

(F–H) Boxplots of learning index in the salt-conditioned WT N2 and transgenic animals, with each dot representing the data from each independent test. Numbers of repeated tests: $n \geq 9$. The statistical significance of difference of SCL behavior in the animals was analyzed by one-way analysis of variance with Tukey's (A, B, and F-H), Dunnett's (C) multiple comparison correction or two-tailed *t* test with unpaired samples (E) and indicated as follows: ns, not significant, $^{*}p < 0.05$, $^{**}p < 0.01$, $^{***}p < 0.001$, and $^{****}p < 0.0001$, and in different colors for varied comparisons. Black: a comparison of tested animals with the WT N2; magenta, a comparison of a gene-rescue transgenic animal vs. the related mutant or as indicated.

and *tyra-2* to answer this issue. ASER in the mock-conditioned *tdc-1*(*n3419*), *tyra-2*(*tm1846*), and RIC:*tdc-1* and ASER:*tyra-2* gene-rescued animals displayed the WT ON- and OFF-responses to the NaCl stimulation. While ASER in the salt-conditioned *tdc-1* and *tyra-2* mutant animals showed obvious ON- and OFF-responses to the NaCl stimulation, there is a significantly reduced sensory plasticity. The ASER Ca^{2+} response and sensory plasticity were restored to the WT phenotypes by the neuron-specific gene-rescue of *tdc-1* in RIC and *tyra-2* in ASER, respectively (Figures 6A–6F). Moreover, the effect of RIC::*TeTx* genetic manipulation on ASER Ca^{2+}-responses to the NaCl stimulation and sensory plasticity fully phenocopied that of *tdc-1* lof mutation (Figures 6G–6I). These results indicate that RIC controls ASER sensory plasticity under salt-conditioning through TA/TYRA-2 signaling.

Based on the SCL phenotype and ASER activity changes, we can deduce that the inhibition of ASER's sensation of NaCl or ASER sensory plasticity is related to SCL. Thus, we analyzed the correlation between ASER's sensory plasticity and animal's learning index in the tested animals, including the WT N2, the mutant, and transgenic animals of *flp-14*, ASER:*flp-14*, *frpr-10*, RIS:*frpr-10*, *pdf-2*, RIS:*pdf-2*, *tdc-1*, RIC:*tdc-1*, *tyra-2*, ASER:*tyra-2*, and RIC::*TeTx*. ASER's sensory plasticity is well fitted with the learning index by linear regression (R squared = 0.8550 and $p < 0.0001$) (Figure 6J). This supports that the ASER's sensory plasticity is positively and directly correlated with the short-term salt chemotaxis learning. Interestingly, ASER's sensory plasticity and the short-term SCL are all-or-none. ASER's sensory plasticity is possibly a cellular mechanism for the short-term SCL.

Our results support that the signaling pathways of FLP-14/FRPR-10 (mediating neurotransmission from ASER to RIS, Figures 3H–3M), PDF-2/PDFR-1 (mediating neurotransmission from RIS to ASER, Figures 4D–4I), and TA/TYRA-2 (mediating neurotransmission from RIC to ASER, Figures 6A–6I), regulate the ASER sensation of NaCl or required for ASER sensory plasticity in SCL. Is there a difference in the effect of these signaling on ASER sensory plasticity? Shown in Figure 6K, the analysis indicates that the ASER sensory plasticity in salt-conditioned mutant animals of *flp-14*, *frpr-10*, *pdf-2*, *pdfr-1*, *tdc-1*, and *tyra-2*, and the transgenic RIC::*TeTx* animal displayed no obvious difference. This supports the idea that all signaling pathways are required for ASER sensory plasticity and that RIC, ASER, and RIS form a circuit to generate the short-term SCL behavior.

Hitherto, this study identifies that sensory neuron ASER and interneurons RIC and RIS play pivot roles in the short-term SCL. What is the role of each neuron in the process of learning

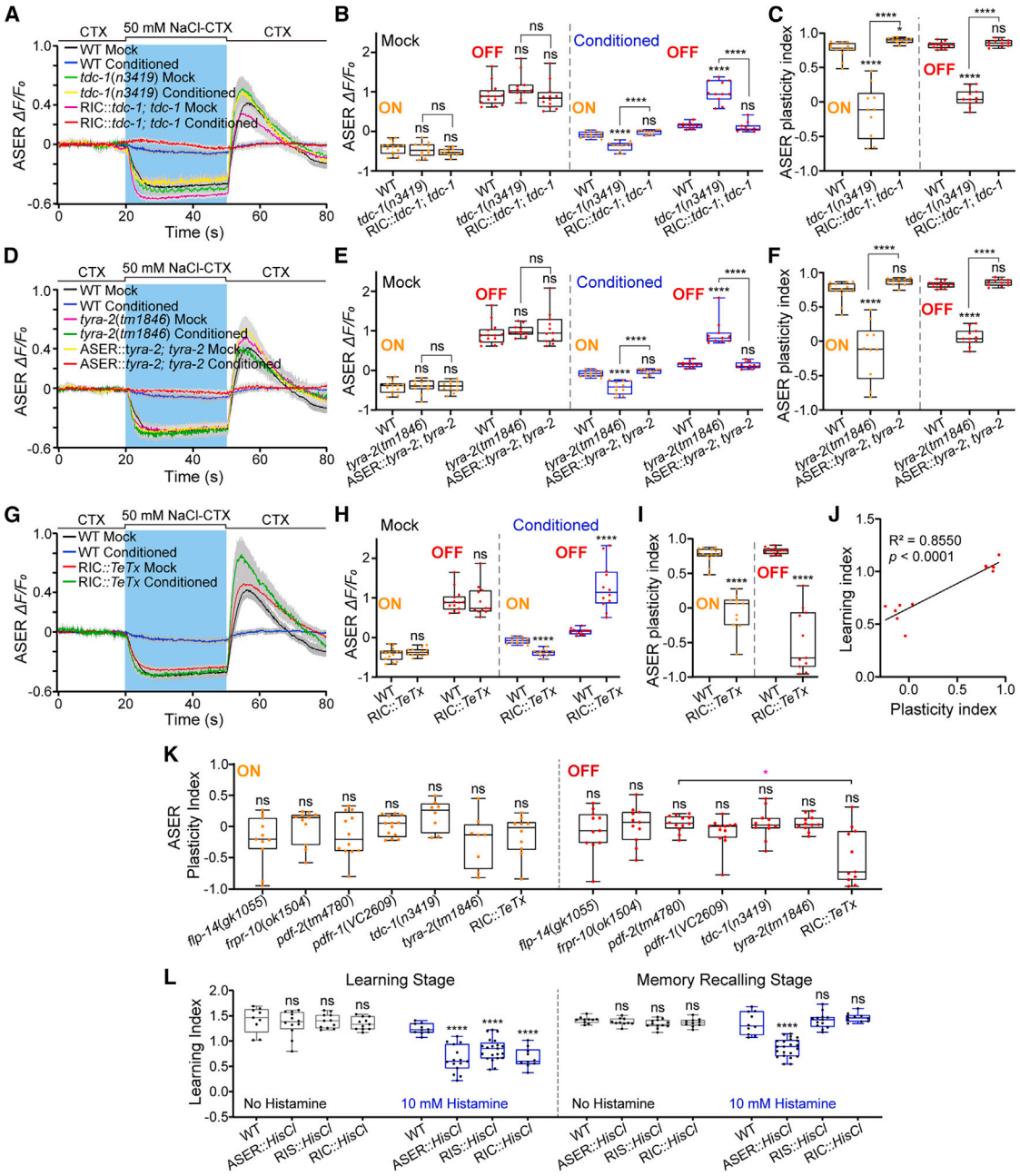

Figure 6. ASER sensory plasticity generated by RIC-ASER-RIS circuit encodes the information of salt chemotaxis learning

(A) Curves of NaCl-induced calcium (Ca^{2+}) responses in ASER neuron in the mock- and salt-conditioned wild-type (WT) N2, *tdc-1*(*n3419*), and RIC:*tdc-1*; *tdc-1* transgenic animals. The Ca^{2+} signals were measured using R-GECO1.0 as a Ca^{2+} indicator and presented as curves of means (solid traces) ± SEM (gray shading), with a light-cyan background indicating the application of 50 mM NaCl/CTX solution. The same hereinafter.

(B) Boxplots of the average intensity of Ca^{2+} signals in the plateau phase (30 s–50 s) of ON response and amplitude of the OFF-response in ASER. The amplitude of the OFF-response was defined as the peak amplitude of the OFF-response minus the average value of ON-response. Each yellow or red dot represents the data of ON- or OFF-responses in each tested animal. The same hereinafter. Numbers of tested animals: $n \geq 11$.

(C) Boxplots of ASER plasticity index in the salt-conditioned WT N2, *tdc-1*(*n3419*), and RIC:*tdc-1*; *tdc-1* transgenic animals. The plasticity index was calculated as $(ON_{mock} - ON_{conditioned})/ON_{mock}$ and $(OFF_{mock} - OFF_{conditioned})/OFF_{mock}$. The same hereinafter.

(D–I) Curves and boxplots of ASER Ca^{2+} responses and plasticity index in the animals of indicated genotypes treated with salt conditioning or mock conditioning. Numbers of tested animals: $n \geq 11$.

(J) Linear correlation between learning index and ASER sensory plasticity index.

(K) Boxplots of ASER sensory plasticity in the animals of indicated genotypes.

(legend continued on next page)

and memory? To answer this issue, we used chemogenetics to acutely inhibit these neurons at the learning or memory-recalling stage by using the cell-specific expression of HisCl1 channels and a treatment of 10 mM histamine. HisCl1 is a histamine-gated chloride channel subunit from *Drosophila* that is effective to tempo-spatially inhibit neurons when activated by exogenous histamine.[71–74,95,96] Our results showed that the chemogenetic inhibition of ASER in both learning and memory recalling stages decreased the learning index of SCL, while the inhibition of RIC or RIS in the learning stage but not in the memory recalling stage reduced SCL ability (Figure 6L). Whereas, the chemogenetic inhibition of all three neurons in the mock-conditioned animals in both learning and memory-recalling stages did not affect chemotaxis to NaCl (Figure S7A). This result indicates that ASER engages in both learning and memory recalling and both RIC and RIS interneurons are involved in only learning but not memory recalling.

The short-term SCL needs about 10 min for the induction of the behavioral plasticity and lasts for about 30 min (Figures S7B and S7C). Our results suggest that ASER sensory plasticity may be a major cause of the short-term SCL behavior. Thus, the time course of ASER sensory plasticity should be like that of the behavior. Indeed, assayed by Ca^{2+} imaging, the salt-conditioning of about 15 min caused significant ASER sensory plasticity. The loss-of-function of TDC-1 and FLP-14 fully suppressed the induction of ASER sensory plasticity (Figures 7A–7E). Moreover, ASER sensory plasticity lasted for about 30 min (Figures 7F–7H). These results support that the time course of ASER sensory plasticity is the same as that of the short-term SCL. In conclusion, all our test results support that ASER sensory plasticity encodes the information of the short-term SCL.

DISCUSSION

Here, we identify a circuital mechanism of short-term SCL. The main salt sensory neuron ASER and interneurons RIC, RIS, and AIY play pivotal roles in the SCL. RIC integrates signals of food availability and NaCl. Under mock conditioning, it releases OA and TA to inhibit AIY and excite ASER through signaling pathways of OCTR-1 on AIY and TYRA-2 on ASER, respectively. While under salt conditioning, RIC activity indicated by Ca^{2+}-response to NaCl stimulation is inhibited. Thus, the RIC suppression of AIY and the augmentation of ASER are depressed by the salt-conditioning. RIC activity plasticity causes behavioral change and ASER sensory plasticity. However, the mechanism for RIC integrating sensory signals and remolding responses to the NaCl stimulation in the salt-conditioned animal needs further study. ASER and RIS form a negative feedback circuit essential for the short-term SCL and ASER sensory plasticity. Under salt conditioning, ASER releases more neuropeptide FLP-14 to augment PDF-2 release in RIS through FRPR-10 signaling, while RIS inhibits the ASER sensation of NaCl via PDF-2/PDFR-1 signaling (Figure 7I).

The inhibition of ASER salt sensation or ASER sensory plasticity generated by salt conditioning encodes the information of short-term salt chemotaxis learning

ASEL and ASER are functionally specialized in NaCl sensation and NaCl chemotaxis.[97–99] ASEL and ASER positively and negatively regulate the chemotaxis to NaCl by augmenting forward locomotion and causing turns, respectively,[99] and differently regulate salt chemotaxis learning with different signaling pathways.[27,100–103] ASER plays a major role in NaCl chemotaxis by both pirouette and weathervane behavioral strategies with ASEL minor contribution. ASE neurons send major synaptic outputs to three interneurons, AIA, AIB, and AIY. Of these, the laser ablation of AIZ caused a severe defect in salt chemotaxis.[104] Laser ablation of ASER but not ASEL reduces chemotaxis to NaCl, while salt conditioning reverses NaCl attraction to NaCl aversion.[104,105]

ASEL shows a robust ON response to the step increases in NaCl concentration from 40 mM to 80 mM and no obvious OFF response to step decreases in NaCl concentration from 40 mM to 0 mM, whereas ASER displays a minor hyperpolarization response to the step increases in NaCl and a robust OFF response to step decreases in NaCl.[99] Thus, ASEL and ASER were recognized as ON and OFF cells of NaCl sensation, respectively. Here, we find that ASER is a both ON- and OFF-cell, with a robust ON-response to step increase of NaCl from 0 mM to 50 mM and an even stronger OFF-response to step decrease of NaCl from 50 mM to 0 mM, under both naïve- and mock-conditioning conditions. Importantly, the ASER Ca^{2+} signals of both ON- and OFF-responses in the salt-conditioned (100 mM NaCl for 20 min) animal were nearly disappeared. Our observation differs from those of previous works.[33,101,106,107] Watteyne et al. focused on ASER OFF-response and observed robust OFF-responses to a 50 to 0 mM NaCl downshift in the mock- and salt-conditioned (100 mM NaCl for 15 min) and an increase of the OFF-response in the salt-conditioned WT N2 animal.[33] Oda et al. observed a similar ASER Ca^{2+} OFF-response to 20 mM–0 mM NaCl downshift and a similar change in OFF-response under salt conditioning (20 mM NaCl for 10 min).[101] Lim et al. observed a transient Ca^{2+} increase in response downshift (20 mM–0 mM) but no ON response to NaCl upshift (0 mM–20 mM) in ASER dendrite in the mock-conditioned WT N2, a minor hyperpolarization ON-response and a decreased OFF-response in the salt-conditioned (20 mM NaCl for 180 min).[106] Dekkers et al. discovered that ASER OFF-responses to NaCl depend on its history of NaCl pre-exposure: shows no response in naive animal and is sensitized by prolonged (at least 30 s) exposure to NaCl in time-dependent manner. Interestingly, ASER sensitization or plasticity is affected by *unc-13* and *eat-4* mutations suggesting that classical neurotransmitter glutamate may engage in ASER sensory plasticity.[107] The observed kinetics difference may be the result of different conditioning and measuring.

Of note, ON- and OFF-responses to NaCl stepwise increase and decrease in ASER in the mock-conditioned animal are

(L) Boxplots of learning index in the animals of salt-conditioned WT N2 and chemogentically inhibited at learning or memory recalling stage. Numbers of repeated tests: $n \geq 10$. The statistical significance of difference was analyzed by one-way analysis of variance with the post hoc test of Dunnett's (H, and L) or Tukey's (B, C, E, F, K) multiple comparison correction, or by two-tailed *t* test with unpaired samples (I), and indicated as follows: ns, not significant, $^{*}p < 0.05$, and $^{****}p < 0.0001$, in comparison with the control (WT N2) or with each other (K).

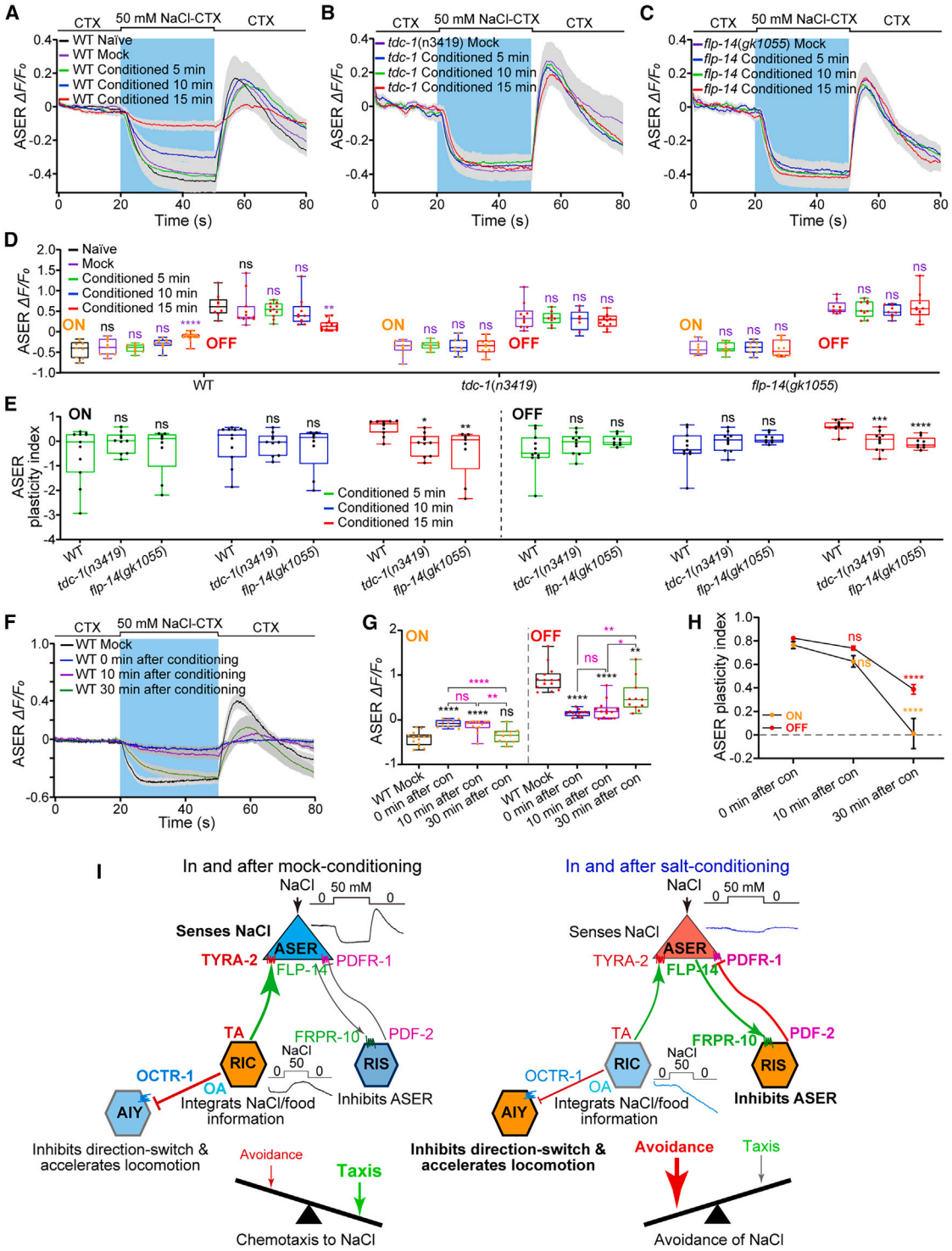

Figure 7. Time course of the ASER sensory plasticity and working model for the mechanism of ASER plasticity and short-term salt chemotaxis learning

(A–C) Curves of ASER Ca^{2+} responses to the NaCl stimulation in wild-type (WT) N2 and mutant animals treated without no conditioning (naive), mock-conditioning of 20 min, and salt-conditioning of varied time (5 min, 10 min, and 15 min).

(D and E) Boxplots of the average intensity of Ca^{2+} signals in the plateau phase (30 s–50 s) of ON response and amplitude of the OFF-response in ASER (D) and ASER sensory plasticity (E) in the indicated animals. Numbers of tested animals: $n \geq 9$.

(legend continued on next page)

hyperpolarization and depolarization. For ASER excitability and activities, especially vesicular release, ON- and OFF-responses are inhibitory and excitatory. Thus, the sensation inhibition or sensory plasticity of these responses are excitatory and inhibitory, respectively. Moreover, ASER ON- and OFF-responses have different dynamics: sustained (or not-decayed) and transient, respectively. Possibly, ON-response is more important than OFF-response in *C. elegans* NaCl chemotaxis. Importantly, our study finds that ASER NaCl-sensation in salt-conditioned animals is almost fully suppressed, that is, salt conditioning causes ASER sensory plasticity. The facts that ASER sensory plasticity is positively and linearly correlated with SCL behavior, it lasts for about 30 min, and chemogenetic inhibiting ASER at both learning and memory stages significantly impairs the short-term SCL (Figures 6 and 7), support that ASER sensory plasticity is required for the behavior. It is reasonable to conclude that the sensory plasticity may encode the information of short-term SCL.

RIC regulates AIY activity and generates ASER sensory plasticity through octopamine and tyramine signaling to generate salt chemotaxis learning

RIC seems to be an interneuron integrating information of external and internal stress and food supply, especially food deprivation, and functions in avoidance behavior, feeding, fat metabolism, and behavioral plasticity.[71,73,85,86,88,90,108] RIC activity is inhibited by food-sensing neuron ADF in a negative correlation manner with food-supply and may synthesize and release both TA and OA[73] TA and OA are invertebrate counterparts of adrenaline and noradrenaline. Adrenergic transmitters function as modulators for metabolism, cellular immune response, the modulation of sensory input, and multiple behaviors, including the fight-or-flight response and L&M.[109] In this study, we identify that RIC releases both TA and OA to regulate AIY interneuron and ASER sensory neuron by acting on OCTR-1 and TYRA-2 receptors, respectively.

RIC Ca^{2+}-response to NaCl stimulation in the salt-conditioned animal was fully suppressed. *tdc-1* in RIC, *octr-1* in AIY, and both TA and OA are required for normal SCL (Figure 5). These indicate that OA from RIC may function to inhibit AIY through OCTR-1 signaling, and AIY inhibition by RIC is reduced when the salt-conditioned animal reencountered NaCl. AIY inhibits the direction-switch by forming an inhibitory circuit with postsynaptic direction-switch promoting interneuron AIZ and promotes locomotion speed by forming an excitatory circuit with RIB.[110] The suppression of RIC inhibition on AIY by salt conditioning found in this study may explain the mechanism of AIY's function in the short-term SCL.

TYRA-2 engages in SCL, as demonstrated in both the report by Moro et al.[25] and this study. Noteworthily, this study revealed that TA/TYRA-2 signaling modulates the ASER sensation of NaCl or causes sensory plasticity in the short-term salt conditioning. Yet, the underlying mechanism remains elusive and needs further study. TYRA-2 is a $G\alpha_{i/o}$-coupled tyramine receptor.[111] Neurohumoral TA from RIM potentiates ASH sensitivity to osmotic stimuli through TYRA-2 signaling.[112] TA/TYRA-2 signaling inhibits RIM activity and mediates feeding suppression by repellent 1-octanol.[113] TYRA-2 is required for avoidance responses to osas#9, an ascaroside pheromone, possibly by acting as a receptor for osas#9,[114] however, sensation modulation by TYRA-2 cannot be excluded.

Neuropeptidergic FLP-14/FRPR-10 and PDF-2/PDFR-1 signaling pathways in the ASER-RIS feedback circuit are required for short-term salt chemotaxis learning

Signaling Pathways of TA/TYRA-2, FLP-14/FRPR-10, and PDF-2/PDFR-1 are equally required for ASER sensory plasticity caused by the salt-conditioning (Figures 6K and 7A–7E). ASER and RIS form a feedback circuit. ASER secretes neurohormone FLP-14, a FMRFamide (Phe-Met-Arg-Phe-NH2)-related peptide, to activate RIS through FRPR-10-GSA-1($G\alpha_s$)-ACY-1(adenylyl cyclase) signaling (Figure S4E). RIS releases neurohumoral PDF-2 acting on PDFR-1 on ASER to inhibit the ASER sensation of NaCl in the salt-conditioned animal. As ASER ON- and OFF-responses are inhibitory and excitatory, respectively, feedback regulation from RIS to ASER may function differently:

(F) Curves and boxplots of ASER Ca^{2+} responses and sensory plasticity index in the mock-conditioned (as the control) and salt-conditioned WT N2 animal at a given time (0 min, 10 min, and 30 min) after the salt-conditioning, respectively.

(G) Boxplots of the average intensity of Ca^{2+} signals in the plateau phase (30 s–50 s) of ON response and amplitude of the OFF-response in ASER in the mock-conditioned (as the control) and salt-conditioned WT N2 animal at a given time (0 min, 10 min, and 30 min) after the salt-conditioning, respectively. Numbers of tested animals: $n \geq 11$.

(H) Curves of ASER plasticity index in the WT N2 animal at different times after salt conditioning. Data were presented as mean ± SEM from more than 10 independent tests. Yellow: plasticity of ON-response; red: plasticity of OFF-response. The statistical significance of difference was analyzed by one-way analysis of variance with the post hoc test of Dunnett's (E) or Tukey's (D and G) multiple comparison correction or two-way analysis of variance with the post hoc test of Sidak's multiple comparisons test (H), and indicated as follows: ns, not significant, $^{*}p < 0.05$, $^{**}p < 0.01$, $^{***}p < 0.001$, and $^{****}p < 0.0001$, and in different colors for varied comparisons. Black: a comparison of tested animals with the WT N2 as a control; purple, a comparison of animals salt-conditioned with different time vs. the mock-conditioned (D); magenta, a comparison of animals at different time (10 min and 30 min) after the salt-conditioning vs. as indicated (G); orange, the plasticity of ON-response at different time (10 min and 30 min) after the salt-conditioning vs. that immediately after conditioning (H); red, the plasticity of OFF-response at different time (10 min and 30 min) after the salt-conditioning vs. that immediately after conditioning (H).

(I) The neuronal circuit generating the short-term salt chemotaxis learning consists of sensory neuron ASER and interneurons of RIC, RIS, and AIY. RIC integrates food-deprivation (or starvation) and salt sensory signals. Upon salt conditioning, RIC Ca^{2+}-response to NaCl stimulation is suppressed. Neurohumoral octopamine and tyramine released by RIC may suppress AIY activity and enlarge the ASER sensation of NaCl through OCTR-1 and TYRA-2 signaling, respectively. The reduced RIC response to NaCl in the salt-conditioned animal weakens RIC actions on ASER and AIY. ASER sensation of NaCl possesses a sustained ON-response of inhibitory hyperpolarization and a transient OFF-response of excitatory depolarization. The inhibition of ASER sensation, or ASER sensory plasticity, facilitates the release of neuropeptide FLP-14. Neuropeptidergic FLP-14/FRPR-10 signaling in RIS augments PDF-2 release. PDF-2/PDFR-1 signaling inhibits ASER salt sensation. The negative feedback by RIS and inhibition by RIC generate ASER sensory plasticity. ASER sensory plasticity and the reduction of AIY inhibition by RIC convert innate salt chemotaxis to learned salt avoidance in *C. elegans*.

augmenting and reducing ASER release of neurotransmitters and modulators in ON and OFF sensory phases, respectively. ASER ON- and OFF-responses may function differently in chemotaxis to NaCl and short-term SCL. This issue needs further study.

FLP-14 is reported to be expressed in multiple neurons, including RID, IL2, and URX.[115–117] This study identifies that FLP-14 expression cells driven by a short *flp-14* promoter of 2 kb are ASE, ASG, and RIS. Among FLP-14 expression neurons, RID releases FLP-14 to promote forward movement in *C. elegans*.[115] Thus, RID may be involved in SCL. However, this study shows that *flp-14* genetic rescue in RID displays no effect (Figure 2A), indicating FLP-14 released from RID does not engage in the short-term SCL.

Mounting evidence support that neuropeptides are important to learning and memory in animals.[118–125] This study discovers that FLP-14/FRRP-10 signaling pathway engages in short-term SCL. Of note, the PDF2/PDFR-1 signaling pathway mediates top-down regulation from interneuron RIS to sensory neuron ASER that is required for ASER sensory plasticity in salt conditioning and short-term SCL.

A neuropeptide may bind with multiple receptors and a neuropeptidergic receptor may bind with multiple neuropeptides. Traditional experimental screen to identify ligand-receptor pairs are labor and time consuming. In identifying receptor(s) of FLP-14 that mediate(s) ASER action on RIS, we used AlphaFold2, a deep-learning-based structure prediction method, to predict potential receptors by modeling ligand-receptor interaction and structure of receptors. AlphaFold2 is useful for the modeling of protein–protein complexes and predicting protein–protein or peptide-protein interaction.[44,46,50,126] Among nineteen predicted potential FLP-14 receptors with the number of ligand-receptor interaction model match ≥ 4, FRPR-10 is a physiological receptor functioning in the short-term SCL. It does not mean other predicted receptors are surely not physiological receptors, they may engage in other functions. The prediction largely narrows our screening scope.

In summary, this study finds that ASER sensory plasticity generated by top-down regulation from RIC and RIS encodes the information of salt chemotaxis learning. Learning and memory, an adaptive behavior plasticity, is based on the physiological and structural plasticity of the nervous system. The plasticity of neurotransmission—long-term potentiation and long-term depression and structural plasticity—formation and maintenance of synapses, pave neuronal basis for long-term learning and memory.[2,3,127] Short-term depression and facilitation of synaptic transmission by sensory neurons mediate short-term habituation and sensitization.[3] Here, we find that the plasticity of Ca^{2+}-responses to NaCl stimulation in sensory neuron caused by top-down regulation is required for the short-term SCL. Since calcium activity reflects any neural activity, including synaptic release, the plasticity of Ca^{2+}-responses presents sensory plasticity. This finding reveals a model for short-term learning and memory.

Limitations of the study

To more physiologically monitor the Ca^{2+} response of ASER and RIC to NaCl stimulation during the short-term salt-chemotaxis learning progress in *C. elegans*, long-term Ca^{2+} imaging in free-moving worms should be needed. However, in this study, short-term Ca^{2+} imaging in immobilized animals was used.

RESOURCE AVAILABILITY

Lead contact

Further information and requests for resources and reagents should be directed to and will be fulfilled by the lead contact, Zheng-Xing Wu (ibbwuzx@mail.hust.edu.cn).

Materials availability

This study did not generate new unique reagents. All worm strains and plasmids used in this study are available to the scientific community. Please email the lead contact.

Data and code availability

- All data reported in this article will be shared by the lead contact on request.
- This article does not report original code.
- Any additional information required to reanalyze the data reported in this article is available from the lead contact on request.

ACKNOWLEDGMENTS

We thank the *Caenorhabditis* Genetic Center (CGC), which is funded by the NIH Office of Research Infrastructure Programs (P40 OD010440), and the National BioResource Project (NBRP) for the worm strains used in this study. This work was supported by grants from the National Natural Science Foundation of China (32071013) and the Fundamental Research Funds for the Central Universities (531119200243).

AUTHOR CONTRIBUTIONS

Z.-X.W. and T.-H.W. supervised the study. P.-Z.W., M.-H.G., and P.S. performed a major part of the experiments, analyzed the data, and created the figures. P.-P.W., L.W., W.Z., Y.X., J.-L.Z., and S.-J.L., R.L., J.-J.W., and H.L performed a minor part of the experiments. Z.-X.W. and P.-Z.W. wrote the article. Y.W. and L.-M.C. assisted with a part of the experimental design. All authors participated in discussions and data interpretation.

DECLARATION OF INTERESTS

The authors declare no competing interests.

STAR★METHODS

Detailed methods are provided in the online version of this paper and include the following:

- KEY RESOURCES TABLE
- EXPERIMENTAL MODEL AND STUDY PARTICIPANT DETAILS
  - Maintenance of worm strains
- METHOD DETAILS
  - Molecular biology
  - Behavioral assays
  - Genetic and chemogenetic manipulations of tested neurons
  - Pharmacological treatment of animals with tyramine and octopamine
  - Calcium imaging
  - Confocal fluorescence imaging
  - Locomotion analysis
  - Neuropeptide-receptor interaction prediction with Alphafold2
  - FRPR-10 expression in *X. laevis* oocytes and whole-cell current recording
- QUANTIFICATION AND STATISTICAL ANALYSIS

SUPPLEMENTAL INFORMATION

Supplemental information can be found online at https://doi.org/10.1016/j.isci.2025.112215.

Received: September 12, 2024
Revised: November 26, 2024
Accepted: March 10, 2025
Published: March 13, 2025

REFERENCES

1. Lieberman, D.A. (2020). Learning and Memory (Cambridge University Press).
2. Kandel, E.R. (2012). The molecular biology of memory: cAMP, PKA, CRE, CREB-1, CREB-2, and CPEB. Mol. Brain *5*, 14. https://doi.org/10.1186/1756-6606-5-14.
3. Kandel, E.R., and LeDoux, J. (2021). Cellular mechanisms of implicit memory storage and the biological basis of individuality. In Principles of Neuronal Science, E.R. Kandel, J.D. Koester, S.H. Mack, and S.A. Siegelbaum, eds. (McGraw Hill), pp. 1312–1338.
4. Owen, G.R., and Brenner, E.A. (2012). Mapping molecular memory: Navigating the cellular pathways of learning. Cell. Mol. Neurobiol. *32*, 919–941. https://doi.org/10.1007/s10571-012-9836-0.
5. Ardiel, E.L., and Rankin, C.H. (2008). Behavioral plasticity in the *C. elegans* mechanosensory circuit. J. Neurogenet. *22*, 239–255. https://doi.org/10.1080/01677060802298509.
6. Sakata, J.T., Catalano, I., and Woolley, S.C. (2022). Mechanisms, development, and comparative perspectives on experience-dependent plasticity in social behavior. J. Exp. Zool. A Ecol. Integr. Physiol. *337*, 35–49. https://doi.org/10.1002/jez.2539.
7. Ishihara, T., Iino, Y., Mohri, A., Mori, I., Gengyo-Ando, K., Mitani, S., and Katsura, I. (2002). HEN-1, a secretory protein with an LDL receptor motif, regulates sensory integration and learning in. Cell *109*, 639–649. https://doi.org/10.1016/S0092-8674(02)00748-1.
8. Sanchez-Alcaniz, J.A., and Benton, R. (2017). Multisensory neural integration of chemical and mechanical signals. Bioessays *39*, 1–11. https://doi.org/10.1002/bies.201700060.
9. Bailey, C.H., and Chen, M. (1988). Long-term sensitization in *Aplysia* increases the number of presynaptic contacts onto the identified gill motor neuron L7. Proc. Natl. Acad. Sci. USA *85*, 9356–9359. https://doi.org/10.1073/pnas.85.23.9356.
10. Bailey, C.H., and Kandel, E.R. (2008). Synaptic remodeling, synaptic growth and the storage of long-term memory in *Aplysia*. Prog. Brain Res. *169*, 179–198. https://doi.org/10.1016/S0079-6123(07)00010-6.
11. Glanzman, D.L. (2009). Habituation in *Aplysia*: the Cheshire cat of neurobiology. Neurobiol. Learn. Mem. *92*, 147–154. https://doi.org/10.1016/j.nlm.2009.03.005.
12. Nikolaev, A., Leung, K.M., Odermatt, B., and Lagnado, L. (2013). Synaptic mechanisms of adaptation and sensitization in the retina. Nat. Neurosci. *16*, 934–941. https://doi.org/10.1038/nn.3408.
13. Bailey, C.H., Kandel, E.R., and Harris, K.M. (2015). Structural Components of Synaptic Plasticity and Memory Consolidation. Cold Spring Harbor Perspect. Biol. *7*, a021758. https://doi.org/10.1101/cshperspect.a021758.
14. McMillen, A., and Chew, Y.L. (2024). Neural mechanisms of dopamine function in learning and memory in *Caenorhabditis elegans*. Neuronal Signal. *8*, NS20230057. https://doi.org/10.1042/NS20230057.
15. Menzel, R., and Benjamin, P.R. (2013). Invertebrate Learning and Memory. In Handbook of Behavioral Neuroscience, R. Menzel and P.R. Benjamin, eds. (Elsevier), pp. 1–603.
16. Rahmani, A., and Chew, Y.L. (2021). Investigating the molecular mechanisms of learning and memory using *Caenorhabditis elegans*. J. Neurochem. *159*, 417–451. https://doi.org/10.1111/jnc.15510.
17. Sasakura, H., and Mori, I. (2013). Behavioral plasticity, learning, and memory in *C. elegans*. Curr. Opin. Neurobiol. *23*, 92–99. https://doi.org/10.1016/j.conb.2012.09.005.
18. White, J.G., Southgate, E., Thomson, J.N., and Brenner, S. (1986). The structure of the nervous system of the *nematode Caenorhabditis elegans*. Philos. Trans. R. Soc. Lond. B Biol. Sci. *314*, 1–340. https://doi.org/10.1098/rstb.1986.0056.
19. Iino, Y. (2013). Salt chemotaxis learning in *Caenorhabditis elegans*. In Invertebrate Learning and Memory, R. Menzel and P.R. Benjamin, eds. (Elsevier Press), pp. 151–159.
20. Hukema, R.K., Rademakers, S., Dekkers, M.P.J., Burghoorn, J., and Jansen, G. (2006). Antagonistic sensory cues generate gustatory plasticity in *Caenorhabditis elegans*. EMBO J. *25*, 312–322. https://doi.org/10.1038/sj.emboj.7600940.
21. Saeki, S., Yamamoto, M., and Iino, Y. (2001). Plasticity of chemotaxis revealed by paired presentation of a chemoattractant and starvation in the *nematode Caenorhabditis elegans*. J. Exp. Biol. *204*, 1757–1764. https://doi.org/10.1242/jeb.204.10.1757.
22. Tomioka, M., Adachi, T., Suzuki, H., Kunitomo, H., Schafer, W.R., and Iino, Y. (2006). The insulin/PI_3-kinase pathway regulates salt chemotaxis learning in *Caenorhabditis elegans*. Neuron *51*, 613–625. https://doi.org/10.1016/j.neuron.2006.07.024.
23. Luo, L., Wen, Q., Ren, J., Hendricks, M., Gershow, M., Qin, Y., Greenwood, J., Soucy, E.R., Klein, M., Smith-Parker, H.K., et al. (2014). Dynamic encoding of perception, memory, and movement in a *C. elegans* chemotaxis circuit. Neuron *82*, 1115–1128. https://doi.org/10.1016/j.neuron.2014.05.010.
24. Zhang, Y., Iino, Y., and Schafer, W.R. (2024). Behavioral plasticity. Genetics *228*, iyae105. https://doi.org/10.1093/genetics/iyae105.
25. Moro, C.A., Sony, S.A., Franklin, L.P., Dong, S., Peifer, M.M., Wittig, K.E., and Hanna-Rose, W. (2023). Adenylosuccinate lyase deficiency affects neurobehavior via perturbations to tyramine signaling in *Caenorhabditis elegans*. PLoS Genet. *19*, e1010974. https://doi.org/10.1371/journal.pgen.1010974.
26. Rosikon, K.D., Bone, M.C., and Lawal, H.O. (2023). Regulation and modulation of biogenic amine neurotransmission in *Drosophila* and *Caenorhabditis elegans*. Front. Physiol. *14*, 970405. https://doi.org/10.3389/fphys.2023.970405.
27. Beets, I., Janssen, T., Meelkop, E., Temmerman, L., Suetens, N., Rademakers, S., Jansen, G., and Schoofs, L. (2012). Vasopressin/oxytocin-related signaling regulates gustatory associative learning in *C. elegans*. Science *338*, 543–545. https://doi.org/10.1126/science.1226860.
28. Chen, Z., Hendricks, M., Cornils, A., Maier, W., Alcedo, J., and Zhang, Y. (2013). Two insulin-like peptides antagonistically regulate aversive olfactory learning in *C. elegans*. Neuron *77*, 572–585. https://doi.org/10.1016/j.neuron.2012.11.025.
29. Kauffman, A.L., Ashraf, J.M., Corces-Zimmerman, M.R., Landis, J.N., and Murphy, C.T. (2010). Insulin signaling and dietary restriction differentially influence the decline of learning and memory with age. PLoS Biol. *8*, e1000372. https://doi.org/10.1371/journal.pbio.1000372.
30. Lee, K., and Mylonakis, E. (2017). An Intestine-Derived Neuropeptide Controls Avoidance Behavior in *Caenorhabditis elegans*. Cell Rep. *20*, 2501–2512. https://doi.org/10.1016/j.celrep.2017.08.053.
31. Lin, C.H.A., Tomioka, M., Pereira, S., Sellings, L., Iino, Y., and van der Kooy, D. (2010). Insulin signaling plays a dual role in *Caenorhabditis elegans* memory acquisition and memory retrieval. J. Neurosci. *30*, 8001–8011. https://doi.org/10.1523/JNEUROSCI.4636-09.2010.
32. Peymen, K., Watteyne, J., Borghgraef, C., Van Sinay, E., Beets, I., and Schoofs, L. (2019). Myoinhibitory peptide signaling modulates aversive gustatory learning in *Caenorhabditis elegans*. PLoS Genet. *15*, e1007945. https://doi.org/10.1371/journal.pgen.1007945.
33. Watteyne, J., Peymen, K., Van der Auwera, P., Borghgraef, C., Vandewyer, E., Van Damme, S., Rutten, I., Lammertyn, J., Jelier, R., Schoofs, L.,

and Beets, I. (2020). Neuromedin U signaling regulates retrieval of learned salt avoidance in a *C. elegans* gustatory circuit. Nat. Commun. *11*, 2076. https://doi.org/10.1038/s41467-020-15964-9.

34. Wu, T., Duan, F., Yang, W., Liu, H., Caballero, A., Fernandes de Abreu, D.A., Dar, A.R., Alcedo, J., Ch'ng, Q., Butcher, R.A., and Zhang, Y. (2019). Pheromones modulate learning by regulating the balanced signals of two insulin-like peptides. Neuron *104*, 1095–1109. https://doi.org/10.1016/j.neuron.2019.09.006.
35. Yamada, K., Hirotsu, T., Matsuki, M., Butcher, R.A., Tomioka, M., Ishihara, T., Clardy, J., Kunitomo, H., and Iino, Y. (2010). Olfactory plasticity is regulated by pheromonal signaling in *Caenorhabditis elegans*. Science *329*, 1647–1650. https://doi.org/10.1126/science.1192020.
36. Koelle, M.R. (2018). Neurotransmitter signaling through heterotrimeric G proteins: insights from studies in *C. elegans* (WormBook), pp. 1–52. https://doi.org/10.1895/wormbook.1.75.2.
37. Jekely, G. (2013). Global view of the evolution and diversity of metazoan neuropeptide signaling. Proc. Natl. Acad. Sci. USA *110*, 8702–8707. https://doi.org/10.1073/pnas.1221833110.
38. Mirabeau, O., and Joly, J.S. (2013). Molecular evolution of peptidergic signaling systems in bilaterians. Proc. Natl. Acad. Sci. USA *110*, E2028–E2037. https://doi.org/10.1073/pnas.1219956110.
39. Van Sinay, E., Mirabeau, O., Depuydt, G., Van Hiel, M.B., Peymen, K., Watteyne, J., Zels, S., Schoofs, L., and Beets, I. (2017). Evolutionarily conserved TRH neuropeptide pathway regulates growth in *Caenorhabditis elegans*. Proc. Natl. Acad. Sci. USA *114*, E4065–E4074. https://doi.org/10.1073/pnas.1617392114.
40. Frooninckx, L., Van Rompay, L., Temmerman, L., Van Sinay, E., Beets, I., Janssen, T., Husson, S.J., and Schoofs, L. (2012). Neuropeptide GPCRs in *C. elegans*. Front. Endocrinol. *3*, 167. https://doi.org/10.3389/fendo.2012.00167.
41. Dagliyan, O., Proctor, E.A., D'Auria, K.M., Ding, F., and Dokholyan, N.V. (2011). Structural and dynamic determinants of protein-peptide recognition. Structure *19*, 1837–1845. https://doi.org/10.1016/j.str.2011.09.014.
42. Johansson-Åkhe, I., Mirabello, C., and Wallner, B. (2019). Predicting protein-peptide interaction sites using distant protein complexes as structural templates. Sci. Rep. *9*, 4267. https://doi.org/10.1038/s41598-019-38498-7.
43. Chang, L., and Perez, A. (2023). Ranking Peptide Binders by Affinity with AlphaFold. Angew. Chem. Int. Ed. Engl. *62*, e202213362. https://doi.org/10.1002/anie.202213362.
44. Humphreys, I.R., Pei, J., Baek, M., Krishnakumar, A., Anishchenko, I., Ovchinnikov, S., Zhang, J., Ness, T.J., Banjade, S., Bagde, S.R., et al. (2021). Computed structures of core eukaryotic protein complexes. Science *374*, eabm4805. https://doi.org/10.1126/science.abm4805.
45. Lin, Z., Akin, H., Rao, R., Hie, B., Zhu, Z., Lu, W., Smetanin, N., Verkuil, R., Kabeli, O., Shmueli, Y., et al. (2023). Evolutionary-scale prediction of atomic-level protein structure with a language model. Science *379*, 1123–1130. https://doi.org/10.1126/science.ade2574.
46. Tsuchiya, Y., Yamamori, Y., and Tomii, K. (2022). Protein-protein interaction prediction methods: from docking-based to AI-based approaches. Biophys. Rev. *14*, 1341–1348. https://doi.org/10.1007/s12551-022-01032-7.
47. Wu, R., Ding, F., Wang, R., Shen, R., Zhang, X., Luo, S., Su, C., Wu, Z., Xie, Q., Berger, B., et al. (2022). High-resolution *de novo* structure prediction from primary sequence. Mendeley Data. https://doi.org/10.1101/2022.07.21.500999.
48. Jumper, J., Evans, R., Pritzel, A., Green, T., Figurnov, M., Ronneberger, O., Tunyasuvunakool, K., Bates, R., Žídek, A., Potapenko, A., et al. (2021). Highly accurate protein structure prediction with AlphaFold. Nature *596*, 583–589. https://doi.org/10.1038/s41586-021-03819-2.
49. Nussinov, R., Zhang, M., Liu, Y., and Jang, H. (2022). AlphaFold, Artificial Intelligence (AI), and Allostery. J. Phys. Chem. B *126*, 6372–6383. https://doi.org/10.1021/acs.jpcb.2c04346.
50. Tsaban, T., Varga, J.K., Avraham, O., Ben-Aharon, Z., Khramushin, A., and Schueler-Furman, O. (2022). Harnessing protein folding neural networks for peptide–protein docking. Nat. Commun. *13*, 176. https://doi.org/10.1038/s41467-021-27838-9.
51. Wicks, S.R., de Vries, C.J., van Luenen, H.G., and Plasterk, R.H. (2000). CHE-3, a cytosolic dynein heavy chain, is required for sensory cilia structure and function in *Caenorhabditis elegans*. Dev. Biol. *221*, 295–307. https://doi.org/10.1006/dbio.2000.9686.
52. Hukema, R.K., Rademakers, S., and Jansen, G. (2008). Gustatory plasticity in *C. elegans* involves integration of negative cues and NaCl taste mediated by serotonin, dopamine, and glutamate. Learn. Mem. *15*, 829–836. https://doi.org/10.1101/lm.994408.
53. Kass, J., Jacob, T.C., Kim, P., and Kaplan, J.M. (2001). The EGL-3 proprotein convertase regulates mechanosensory responses of *Caenorhabditis elegans*. J. Neurosci. *21*, 9265–9272. https://doi.org/10.1523/JNEUROSCI.21-23-09265.2001.
54. Van Bael, S., Watteyne, J., Boonen, K., De Haes, W., Menschaert, G., Ringstad, N., Horvitz, H.R., Schoofs, L., Husson, S.J., and Temmerman, L. (2018). Mass spectrometric evidence for neuropeptide-amidating enzymes in *Caenorhabditis elegans*. J. Biol. Chem. *293*, 6052–6063. https://doi.org/10.1074/jbc.RA117.000731.
55. Van Bael, S., Zels, S., Boonen, K., Beets, I., Schoofs, L., and Temmerman, L. (2018). A *Caenorhabditis elegans* mass spectrometric resource for neuropeptidomics. J. Am. Soc. Mass Spectrom. *29*, 879–889. https://doi.org/10.1007/s13361-017-1856-z.
56. Li, W., Kennedy, S.G., and Ruvkun, G. (2003). *daf-28* encodes a *C. elegans* insulin superfamily member that is regulated by environmental cues and acts in the DAF-2 signaling pathway. Gene Dev. *17*, 844–858. https://doi.org/10.1101/gad.1066503.
57. Pierce, S.B., Costa, M., Wisotzkey, R., Devadhar, S., Homburger, S.A., Buchman, A.R., Ferguson, K.C., Heller, J., Platt, D.M., Pasquinelli, A.A., et al. (2001). Regulation of DAF-2 receptor signaling by human insulin and *ins-1*, a member of the unusually large and diverse *C. elegans* insulin gene family. Genes Dev. *15*, 672–686. https://doi.org/10.1101/gad.867301.
58. Li, C., Kim, K., and Nelson, L.S. (1999). FMRFamide-related neuropeptide gene family in *Caenorhabditis elegans*. Brain Res. *848*, 26–34. https://doi.org/10.1016/s0006-8993(99)01972-1.
59. Nathoo, A.N., Moeller, R.A., Westlund, B.A., and Hart, A.C. (2001). Identification of neuropeptide-like protein gene families in *Caenorhabditis elegans* and other species. Proc. Natl. Acad. Sci. USA *98*, 14000–14005. https://doi.org/10.1073/pnas.241231298.
60. Li, C., and Kim, K. (2008). Neuropeptides (WormBook), pp. 1–36. https://doi.org/10.1895/wormbook.1.142.1.
61. Gershkovich, M.M., Groß, V.E., Kaiser, A., and Prömel, S. (2019). Pharmacological and functional similarities of the human neuropeptide Y system in *C. elegans* challenges phylogenetic views on the FLP/NPR system. Cell Commun. Signal. *17*, 123. https://doi.org/10.1186/s12964-019-0436-1.
62. Marques, F., Falquet, L., Vandewyer, E., Beets, I., and Glauser, D.A. (2021). Signaling via the FLP-14/FRPR-19 neuropeptide pathway sustains nociceptive response to repeated noxious stimuli in *C. elegans*. PLoS Genet. *17*, e1009880. https://doi.org/10.1371/journal.pgen.1009880.
63. Beets, I., Zels, S., Vandewyer, E., Demeulemeester, J., Caers, J., Baytemur, E., Courtney, A., Golinelli, L., Hasakioğulları, İ., Schafer, W.R., et al. (2023). System-wide mapping of peptide-GPCR interactions in *C. elegans*. Cell Rep. *42*, 113058. https://doi.org/10.1016/j.celrep.2023.113058.
64. Bryant, P., Pozzati, G., and Elofsson, A. (2022). Improved prediction of protein-protein interactions using AlphaFold2. Nat. Commun. *13*, 1265. https://doi.org/10.1038/s41467-022-28865-w.

65. Danneskiold-Samsøe, N.B., Kavi, D., Jude, K.M., Nissen, S.B., Wat, L.W., Coassolo, L., Zhao, M., Santana-Oikawa, G.A., Broido, B.B., and Garcia, K.C. (2023). Rapid and accurate deorphanization of ligand–receptor pairs using AlphaFold. Mendeley Data. https://doi.org/10.1101/2023.03.16.531341.

66. Kishore, R., Arnaboldi, V., Van Slyke, C.E., Chan, J., Nash, R.S., Urbano, J.M., Dolan, M.E., Engel, S.R., Shimoyama, M., Sternberg, P.W., and Genome Resources, T.A.O. (2020). Automated generation of gene summaries at the Alliance of Genome Resources. Database *2020*, baaa037. https://doi.org/10.1093/database/baaa037.

67. Ringstad, N., and Horvitz, H.R. (2008). FMRFamide neuropeptides and acetylcholine synergistically inhibit egg-laying by *C. elegans*. Nat. Neurosci. *11*, 1168–1176. https://doi.org/10.1038/nn.2186.

68. Rogers, C., Reale, V., Kim, K., Chatwin, H., Li, C., Evans, P., and de Bono, M. (2003). Inhibition of *Caenorhabditis elegans* social feeding by FMRFamide-related peptide activation of NPR-1. Nat. Neurosci. *6*, 1178–1185. https://doi.org/10.1038/nn1140.

69. Schiavo, G., Benfenati, F., Poulain, B., Rossetto, O., Polverino de Laureto, P., DasGupta, B.R., and Montecucco, C. (1992). Tetanus and botulinum-B neurotoxins block neurotransmitter release by proteolytic cleavage of synaptobrevin. Nature *359*, 832–835. https://doi.org/10.1038/359832a0.

70. Guo, M., Ge, M., Berberoglu, M.A., Zhou, J., Ma, L., Yang, J., Dong, Q., Feng, Y., Wu, Z., and Dong, Z. (2018). Dissecting molecular and circuit mechanisms for inhibition and delayed response of ASI neurons during nociceptive stimulus. Cell Rep. *25*, 1885–1897. https://doi.org/10.1016/j.celrep.2018.10.065.

71. Guo, M., Wu, T.H., Song, Y.X., Ge, M.H., Su, C.M., Niu, W.P., Li, L.L., Xu, Z.J., Ge, C.L., Al-Mhanawi, M.T.H., et al. (2015). Reciprocal inhibition between sensory ASH and ASI neurons modulates nociception and avoidance in *Caenorhabditis elegans*. Nat. Commun. *6*, 5655. https://doi.org/10.1038/Ncomms6655.

72. Li, R., Xu, Y., Wen, X., Chen, Y.H., Wang, P.Z., Zhao, J.L., Wu, P.P., Wu, J.J., Liu, H., Huang, J.H., et al. (2024). GCY-20 signaling controls suppression of *Caenorhabditis elegans* egg laying by moderate cold. Cell Rep. *43*, 113708. https://doi.org/10.1016/j.celrep.2024.113708.

73. Liu, H., Qin, L.W., Li, R., Zhang, C., Al-Sheikh, U., and Wu, Z.X. (2019). Reciprocal modulation of 5-HT and octopamine regulates pumping via feedforward and feedback circuits in *C. elegans*. Proc. Natl. Acad. Sci. USA *116*, 7107–7112. https://doi.org/10.1073/pnas.1819261116.

74. Liu, H., Wu, J.J., Li, R., Wang, P.Z., Huang, J.H., Xu, Y., Zhao, J.L., Wu, P.P., Li, S.J., and Wu, Z.X. (2023). Disexcitation in the ASH/RIM/ADL negative feedback circuit fine-tunes hyperosmotic sensation and avoidance in *Caenorhabditis elegans*. Front. Mol. Neurosci. *16*, 1101628. https://doi.org/10.3389/fnmol.2023.1101628.

75. Macosko, E.Z., Pokala, N., Feinberg, E.H., Chalasani, S.H., Butcher, R.A., Clardy, J., and Bargmann, C.I. (2009). A hub-and-spoke circuit drives pheromone attraction and social behaviour in *C. elegans*. Nature *458*, 1171–1175. https://doi.org/10.1038/nature07886.

76. Wen, X., Chen, Y.H., Li, R., Ge, M.H., Yin, S.W., Wu, J.J., Huang, J.H., Liu, H., Wang, P.Z., Gross, E., and Wu, Z.X. (2020). Signal decoding for glutamate modulating egg laying oppositely in *Caenorhabditis elegans* under varied environmental conditions. iScience *23*, 101588. https://doi.org/10.1016/j.isci.2020.101588.

77. Bastiani, C., and Mendel, J. (2006). Heterotrimeric G Proteins in *C. elegans* (WormBook), pp. 1–25. https://doi.org/10.1895/wormbook.1.75.1.

78. Jin, Y., Jorgensen, E., Hartwieg, E., and Horvitz, H.R. (1999). The *Caenorhabditis elegans* gene *unc-25* encodes glutamic acid decarboxylase and is required for synaptic transmission but not synaptic development. J. Neurol. Sci. *19*, 539–548. https://doi.org/10.1523/JNEUROSCI.19-02-00539.1999.

79. Janssen, T., Husson, S.J., Meelkop, E., Temmerman, L., Lindemans, M., Verstraelen, K., Rademakers, S., Mertens, I., Nitabach, M., Jansen, G., and Schoofs, L. (2009). Discovery and characterization of a conserved pigment dispersing factor-like neuropeptide pathway in *Caenorhabditis elegans*. J. Neurochem. *111*, 228–241. https://doi.org/10.1111/j.1471-4159.2009.06323.x.

80. Cook, S.J., Jarrell, T.A., Brittin, C.A., Wang, Y., Bloniarz, A.E., Yakovlev, M.A., Nguyen, K.C.Q., Tang, L.T.H., Bayer, E.A., Duerr, J.S., et al. (2019). Whole-animal connectomes of both *Caenorhabditis elegans* sexes. Nature *571*, 63–71. https://doi.org/10.1038/s41586-019-1352-7.

81. Altun, Z.F., Chen, B., Wang, Z.W., and Hall, D.H. (2009). High resolution map of *Caenorhabditis elegans* gap junction proteins. Dev. Dyn. *238*, 1936–1950. https://doi.org/10.1002/dvdy.22025.

82. Durham, T.J., Daza, R.M., Gevirtzman, L., Cusanovich, D.A., Bolonduro, O., Noble, W.S., Shendure, J., and Waterston, R.H. (2021). Comprehensive characterization of tissue-specific chromatin accessibility in L2 *Caenorhabditis elegans nematodes*. Genome Res. *31*, 1952–1969. https://doi.org/10.1101/gr.271791.120.

83. Lockhead, D., Schwarz, E.M., O'Hagan, R., Bellotti, S., Krieg, M., Barr, M.M., Dunn, A.R., Sternberg, P.W., and Goodman, M.B. (2016). The tubulin repertoire of *Caenorhabditis elegans* sensory neurons and its context-dependent role in process outgrowth. Mol. Biol. Cell *27*, 3717–3728. https://doi.org/10.1091/mbc.E16-06-0473.

84. Meelkop, E., Temmerman, L., Janssen, T., Suetens, N., Beets, I., Van Rompay, L., Shanmugam, N., Husson, S.J., and Schoofs, L. (2012). PDF receptor signaling in *Caenorhabditis elegans* modulates locomotion and egg-laying. Mol. Cell. Endocrinol. *361*, 232–240. https://doi.org/10.1016/j.mce.2012.05.001.

85. Greer, E.R., Pérez, C.L., Van Gilst, M.R., Lee, B.H., and Ashrafi, K. (2008). Neural and molecular dissection of a *C. elegans* sensory circuit that regulates fat and feeding. Cell Metab. *8*, 118–131. https://doi.org/10.1016/j.cmet.2008.06.005.

86. Lemieux, G.A., Cunningham, K.A., Lin, L., Mayer, F., Werb, Z., and Ashrafi, K. (2015). Kynurenic acid is a nutritional cue that enables behavioral plasticity. Cell *160*, 119–131. https://doi.org/10.1016/j.cell.2014.12.028.

87. Li, Z., Li, Y., Yi, Y., Huang, W., Yang, S., Niu, W., Zhang, L., Xu, Z., Qu, A., Wu, Z., and Xu, T. (2012). Dissecting a central flip-flop circuit that integrates contradictory sensory cues in *C. elegans* feeding regulation. Nat. Commun. *3*, 776. https://doi.org/10.1038/ncomms1780.

88. Liao, C.P., Chiang, Y.C., Tam, W.H., Chen, Y.J., Chou, S.H., and Pan, C.L. (2022). Neurophysiological basis of stress-induced aversive memory in the nematode *Caenorhabditis elegans*. Curr. Biol. *32*, 5309–5322. https://doi.org/10.1016/j.cub.2022.11.012.

89. Liu, M., Xiong, Y., Shan, S., Zhu, Y., Zeng, D., Shi, Y., Zhang, Y., and Lu, W. (2020). Eleutheroside E enhances the long-term memory of radiation-damaged *C. elegans* through G-protein-coupled receptor and neuropeptide signaling pathways. J. Nat. Prod. *83*, 3315–3323. https://doi.org/10.1021/acs.jnatprod.0c00650.

90. Noble, T., Stieglitz, J., and Srinivasan, S. (2013). An integrated serotonin and octopamine neuronal circuit directs the release of an endocrine signal to control *C. elegans* body fat. Cell Metab. *18*, 672–684. https://doi.org/10.1016/j.cmet.2013.09.007.

91. Tao, J., Ma, Y.C., Yang, Z.S., Zou, C.G., and Zhang, K.Q. (2016). Octopamine connects nutrient cues to lipid metabolism upon nutrient deprivation. Sci. Adv. *2*, e1501372. https://doi.org/10.1126/sciadv.1501372.

92. Suo, S., Culotti, J.G., and Van Tol, H.H.M. (2009). Dopamine counteracts octopamine signalling in a neural circuit mediating food response in *C. elegans*. EMBO J. *28*, 2437–2448. https://doi.org/10.1038/emboj.2009.194.

93. Suo, S., Kimura, Y., and Van Tol, H.H.M. (2006). Starvation induces cAMP response element-binding protein-dependent gene expression through octopamine-Gq signaling in *Caenorhabditis elegans*. J. Neurosci. *26*, 10082–10090. https://doi.org/10.1523/JNEUROSCI.0819-06.2006.

94. Alkema, M.J., Hunter-Ensor, M., Ringstad, N., and Horvitz, H.R. (2005). Tyramine functions independently of octopamine in the *Caenorhabditis elegans* nervous system. Neuron *46*, 247–260. https://doi.org/10.1016/j.neuron.2005.02.024.

95. Pokala, N., Liu, Q., Gordus, A., and Bargmann, C.I. (2014). Inducible and titratable silencing of *Caenorhabditis elegans* neurons *in vivo* with histamine-gated chloride channels. Proc. Natl. Acad. Sci. USA *111*, 2770–2775. https://doi.org/10.1073/pnas.1400615111.

96. Wu, J.J., Yin, S.W., Liu, H., Li, R., Huang, J.H., Wang, P.Z., Xu, Y., Zhao, J.L., Wu, P.P., and Wu, Z.X. (2022). Positive interaction between ASH and ASK sensory neurons accelerates nociception and inhibits behavioral adaptation. iScience *25*, 105287. https://doi.org/10.1016/j.isci.2022.105287.

97. Bargmann, C.I. (2006). Chemosensation in *C. elegans* (WormBook), pp. 1–29. https://doi.org/10.1895/wormbook.1.123.1.

98. Pierce-Shimomura, J.T., Faumont, S., Gaston, M.R., Pearson, B.J., and Lockery, S.R. (2001). The homeobox gene lim-6 is required for distinct chemosensory representations in *C. elegans*. Nature *410*, 694–698. https://doi.org/10.1038/35070575.

99. Suzuki, H., Thiele, T.R., Faumont, S., Ezcurra, M., Lockery, S.R., and Schafer, W.R. (2008). Functional asymmetry in *Caenorhabditis elegans* taste neurons and its computational role in chemotaxis. Nature *454*, 114–117. https://doi.org/10.1038/nature06927.

100. Adachi, T., Kunitomo, H., Tomioka, M., Ohno, H., Okochi, Y., Mori, I., and Iino, Y. (2010). Reversal of salt preference is directed by the insulin/PI3K and G_q/PKC signaling in *Caenorhabditis elegans*. Genetics *186*, 1309–1319. https://doi.org/10.1534/genetics.110.119768.

101. Oda, S., Tomioka, M., and Iino, Y. (2011). Neuronal plasticity regulated by the insulin-like signaling pathway underlies salt chemotaxis learning in *Caenorhabditis elegans*. J. Neurophysiol. *106*, 301–308. https://doi.org/10.1152/jn.01029.2010.

102. Ohno, H., Kato, S., Naito, Y., Kunitomo, H., Tomioka, M., and Iino, Y. (2014). Role of synaptic phosphatidylinositol 3-kinase in a behavioral learning response in *C. elegans*. Science *345*, 313–317. https://doi.org/10.1126/science.1250709.

103. Tomioka, M., Naito, Y., Kuroyanagi, H., and Iino, Y. (2016). Splicing factors control *C. elegans* behavioural learning in a single neuron by producing DAF-2c receptor. Nat. Commun. *7*, 11645. https://doi.org/10.1038/ncomms11645.

104. Iino, Y., and Yoshida, K. (2009). Parallel use of two behavioral mechanisms for chemotaxis in *Caenorhabditis elegans*. J. Neurosci. *29*, 5370–5380. https://doi.org/10.1523/Jneurosci.3633-08.2009.

105. Pierce-Shimomura, J.T., Morse, T.M., and Lockery, S.R. (1999). The fundamental role of pirouettes in *Caenorhabditis elegans* chemotaxis. J. Neurosci. *19*, 9557–9569. https://doi.org/10.1523/JNEUROSCI.19-21-09557.1999.

106. Lim, J.P., Fehlauer, H., Das, A., Saro, G., Glauser, D.A., Brunet, A., and Goodman, M.B. (2018). Loss of CaMKI function disrupts salt aversive learning in *C. elegans*. J. Neurosci. *38*, 6114–6129. https://doi.org/10.1523/JNEUROSCI.1611-17.2018.

107. Dekkers, M.P.J., Salfelder, F., Sanders, T., Umuerri, O., Cohen, N., and Jansen, G. (2021). Plasticity in gustatory and nociceptive neurons controls decision making in *C. elegans* salt navigation. Commun. Biol. *4*, 1053. https://doi.org/10.1038/s42003-021-02561-9.

108. Kimura, K.D., Fujita, K., and Katsura, I. (2010). Enhancement of odor avoidance regulated by dopamine signaling in *Caenorhabditis elegans*. J. Neurosci. *30*, 16365–16375. https://doi.org/10.1523/Jneurosci.6023-09.2010.

109. Roeder, T. (2005). Tyramine and octopamine: Ruling behavior and metabolism. Annu. Rev. Entomol. *50*, 447–477. https://doi.org/10.1146/annurev.ento.50.071803.130404.

110. Li, Z., Liu, J., Zheng, M., and Xu, X.Z.S. (2014). Encoding of both analog- and digital-like behavioral outputs by one *C. elegans* interneuron. Cell *159*, 751–765. https://doi.org/10.1016/j.cell.2014.09.056.

111. Rex, E., Hapiak, V., Hobson, R., Smith, K., Xiao, H., and Komuniecki, R. (2005). TYRA-2 (F01E11.5): A *Caenorhabditis elegans* tyramine receptor expressed in the MC and NSM pharyngeal neurons. J. Neurochem. *94*, 181–191. https://doi.org/10.1111/j.1471-4159.2005.03180.x.

112. Ghosh, D.D., Sanders, T., Hong, S., McCurdy, L.Y., Chase, D.L., Cohen, N., Koelle, M.R., and Nitabach, M.N. (2016). Neural architecture of hunger-dependent multisensory decision making in *C. elegans*. Neuron *92*, 1049–1062. https://doi.org/10.1016/j.neuron.2016.10.030.

113. Fu, J., Zhang, H., Huang, W., Zhu, X., Sheng, Y., Song, E., and Xu, T. (2018). AIM interneurons mediate feeding suppression through the TYRA-2 receptor in *C. elegans*. Biophys. Rep. *4*, 17–24. https://doi.org/10.1007/s41048-018-0046-2.

114. Chute, C.D., DiLoreto, E.M., Zhang, Y.K., Reilly, D.K., Rayes, D., Coyle, V.L., Choi, H.J., Alkema, M.J., Schroeder, F.C., and Srinivasan, J. (2019). Co-option of neurotransmitter signaling for inter-organismal communication in *C. elegans*. Nat. Commun. *10*, 3186. https://doi.org/10.1038/s41467-019-11240-7.

115. Lim, M.A., Chitturi, J., Laskova, V., Meng, J., Findeis, D., Wiekenberg, A., Mulcahy, B., Luo, L., Li, Y., Lu, Y., et al. (2016). Neuroendocrine modulation sustains the *C. elegans* forward motor state. Elife *5*, e19887. https://doi.org/10.7554/eLife.19887.

116. Sun, H., and Hobert, O. (2021). Temporal transitions in the post-mitotic nervous system of *Caenorhabditis elegans*. Nature *600*, 93–99. https://doi.org/10.1038/s41586-021-04071-4.

117. Taylor, S.R., Santpere, G., Weinreb, A., Barrett, A., Reilly, M.B., Xu, C., Varol, E., Oikonomou, P., Glenwinkel, L., McWhirter, R., et al. (2021). Molecular topography of an entire nervous system. Cell *184*, 4329–4347. https://doi.org/10.1016/j.cell.2021.06.023.

118. Borbely, E., Scheich, B., and Helyes, Z. (2013). Neuropeptides in learning and memory. Neuropeptides *47*, 439–450. https://doi.org/10.1016/j.npep.2013.10.012.

119. Del Pino, I., Brotons-Mas, J.R., Marques-Smith, A., Marighetto, A., Frick, A., Marín, O., and Rico, B. (2017). Abnormal wiring of CCK(+) basket cells disrupts spatial information coding. Nat. Neurosci. *20*, 784–792. https://doi.org/10.1038/nn.4544.

120. Krashes, M.J., DasGupta, S., Vreede, A., White, B., Armstrong, J.D., and Waddell, S. (2009). A neural circuit mechanism integrating motivational state with memory expression in *Drosophila*. Cell *139*, 416–427. https://doi.org/10.1016/j.cell.2009.08.035.

121. Ma, S., Hangya, B., Leonard, C.S., Wisden, W., and Gundlach, A.L. (2018). Dual-transmitter systems regulating arousal, attention, learning and memory. Neurosci. Biobehav. Rev. *85*, 21–33. https://doi.org/10.1016/j.neubiorev.2017.07.009.

122. Marquina-Solis, J., Feng, L., Vandewyer, E., Beets, I., Hawk, J., Colón-Ramos, D.A., Yu, J., Fox, B.W., Schroeder, F.C., and Bargmann, C.I. (2024). Antagonism between neuropeptides and monoamines in a distributed circuit for pathogen avoidance. Cell Rep. *43*, 114042. https://doi.org/10.1016/j.celrep.2024.114042.

123. Rangel Guerrero, D.K., Balueva, K., Barayeu, U., Baracskay, P., Gridchyn, I., Nardin, M., Roth, C.N., Wulff, P., and Csicsvari, J. (2024). Hippocampal cholecystokinin-expressing interneurons regulate temporal coding and contextual learning. Neuron *112*, 2045–2061. https://doi.org/10.1016/j.neuron.2024.03.019.

124. Varas, M.M., Pérez, M.F., Ramírez, O.A., and de Barioglio, S.R. (2003). Increased susceptibility to LTP generation and changes in NMDA-NR1 and -NR2B subunits mRNA expression in rat hippocampus after MCH administration. Peptides *24*, 1403–1411. https://doi.org/10.1016/j.peptides.2003.09.006.

125. Wang, C., Xin, L., Cai, C.C., Cong, C.Y., Xie, J.F., Kong, X.P., Dong, C.Y., Li, J., Cui, G.F., Chen, H.L., et al. (2020). Neuropeptide S displays as a key neuromodulator in olfactory spatial memory. Chem. Senses *45*, 195–202. https://doi.org/10.1093/chemse/bjaa003.

126. Burke, D.F., Bryant, P., Barrio-Hernandez, I., Memon, D., Pozzati, G., Shenoy, A., Zhu, W., Dunham, A.S., Albanese, P., Keller, A., et al. (2023). Towards a structurally resolved human protein interaction network. Nat. Struct. Mol. Biol. *30*, 216–225. https://doi.org/10.1038/s41594-022-00910-8.

127. Ardiel, E.L., and Rankin, C.H. (2010). An elegant mind: learning and memory in *Caenorhabditis elegans*. Learn. Mem. *17*, 191–201. https://doi.org/10.1101/lm.960510.

128. Mello, C.C., Kramer, J.M., Stinchcomb, D., and Ambros, V. (1991). Efficient gene transfer in *C. elegans*: Extrachromosomal maintenance and integration of transforming sequences. EMBO J. *10*, 3959–3970. https://doi.org/10.1002/j.1460-2075.1991.tb04966.x.

129. Brenner, S. (1974). The genetics of *Caenorhabditis elegans*. Genetics *77*, 71–94. https://doi.org/10.1093/genetics/77.1.71.

STAR★METHODS

KEY RESOURCES TABLE

REAGENT or RESOURCE	SOURCE	IDENTIFIER
Bacterial and virus strains		
Escherichia coli OP50	Caenorhabditis Genetics Center	WB Cat# WBStrain00041969
Chemicals, peptides, and recombinant proteins		
Agar	Sigma-Aldrich	Cat#V900500; CAS: 9002-18-0
Potassium phosphate dibasic trihydrate ($K_2HPO_4 \cdot 3H_2O$)	Sigma-Aldrich	Cat#10017518; CAS: 16788-57-1
Potassium phosphate monobasic (KH_2PO_4)	Sinopharm Chemical Reagent	Cat#10017618; CAS: 7778-77-0
Yeast Extract	Thermo Scientific™	Cat#LP0021B CAS: 8013-01-2
Bacto™ Peptone	Gibco™	Cat#211677; CAS: 73049-73-7
Tryptone	Thermo Scientific™	Cat#LP0042B; CAS: 91079-40-2
Histamine dihydrochloride	Sigma-Aldrich	Cat#V900411; CAS: 56-92-8
Agarose Gel DNA Extraction Kit	GENEray biotech	Cat#GK2043-50
TIANpure Midi Plasmid Kit	YIANGEN	Cat#DP107-02
Gateway™ BP Clonase™ II Enzyme Mix	Thermo Scientific™	Cat#11789100
Gateway™ LR Clonase™ II Plus Enzyme Mix	Thermo Scientific™	Cat#11791100
ClonExpressII One Step Cloning Kit	Vazyme Biotech co., ltd	Vazyme#C112
FLP-14	Guoping Pharmaceutical Company	KHEYLRFG-NH_2
Experimental models: Organisms/strains		
C. elegans strain, see Table S2	This paper	N/A
Oligonucleotides		
See Table S3	This paper	N/A
Recombinant DNA		
See Table S4	This paper	N/A
Software and algorithms		
ImageJ	National Institutes of Health	https://imagej.nih.gov/ij/
SnapGene	Insightful Science	https://www.snapgene.com
MATLAB R2019a	MathWorks	https://www.mathworks.com/help/matlab/release-notes-R2019a.html
Image Pro Plus 6.0	Media Cybernetics	https://mediacy.com/image-pro
Igor Pro 6.10	WaveMetrics	https://www.wavemetrics.com
GraphPad Prism 9.5	GraphPad Software Inc.	https://www.graphpad.com
Clampfit	Molecular Devices	https://www.moleculardevices.com
Clampex 8.0	Molecular Devices	https://www.moleculardevices.com
MEGA 6.60	Molecular Evolutionary Genetics Analysis	https://megasoftware.net

EXPERIMENTAL MODEL AND STUDY PARTICIPANT DETAILS

Maintenance of worm strains

All *C. elegans* strains were cultured on nematode growth media (NGM) plates at 20°C using *E. coli* bacteria OP50 as food by standard procedures. The strains were obtained from the CGC (http://www.cbs.umn.edu/CGC/) or the National Bio-Resources Project (NBRP, http://www.shigen.nig.ac.jp/c.elegans/indices.jsp). All transgenic animals were generated with standard microinjection techniques.[128] The most plasmids were injected at 50 ng/μL together with *lin-44p*::*GFP* or *vha-6p*::*GFP* as a coinjection marker at 10 ng/μL. The injection pressure was controlled by a DMP-300 digital pneumatic microinjection pump (Micrology Precision Instruments, Ltd, Wuhan, China). The double mutant animals were generated using the standard genetic techniques,[129] and confirmed by PCR and sequencing. The strain of *frpr-10*(*ok1504*) was backcrossed to the wild-type (WT) N2 five times to remove unlinked mutations. The strain of *flp-14*(*gk1055*) was backcrossed to the WT N2 five times to remove *sfxn1.2* mutation. Additionally, the allocation of animals to experimental groups followed a random assignment procedure, ensuring an unbiased and rigorous experimental design. For microbe strains, we used Escherichia coli OP50 as the food of *C. elegans* after culturing it in nematode growth medium (NGM) plates at 37C for 8 h. This bacterial strain could be from the Caenorhabditis Genetics Center with the WormBase ID (WBStrain00041969). All animals used in this study are listed in key resources table.

METHOD DETAILS

Molecular biology

Construction of expression plasmids

All expression plasmids used in this study were constructed by Three-Fragment Multisite® gateway system (Invitrogen™, Thermo Fisher Scientific, Waltham, MA, USA). Briefly, three entry clones, A, B and C, comprising three PCR products (promoter, the gene of interest, and *sl2::TagRFP-t* or 3' UTR, respectively) were recombined into the pDEST™ R4-R3 Vector II (from Addgene, http://www.addgene.org/vector-database) or custom-modified destination vectors pDEST-R4-R3-*unc-54* 3'UTR or pBCN44-R4-R3-*lin-44p*::*GFP*, using *att*L-*att*R (LR) recombination reactions to generate expression clones. pDEST-R4-R3-*unc-54 3'*UTR destination vector was modified from the pDEST-R4-R3 vector by inserting *unc-54 3'* UTR at the position between *att*R3 and *AmpR* promoter, with PCR-linearization and In-fusion methods. pBCN44-R4-R3-*lin-44p*::*GFP* destination vectors was modified from the pBCN44-R4-R3 vector by inserting *lin-44p*::GFP serving as a gene marker for transgene into the backbone with restriction enzyme digestion method.

Construction of an entry clone A containing a promoter

An entry clone A contributing sequence of slot 1 in the expression plasmid contains sequence of a promoter. We used an In-Fusion method or BP reaction to construct them. With the In-Fusion method, we used a promoter sequence to substitute for promoter fragment in an entry clone A used in LR reactions in Three-Fragment Multisite gateway system. In brief, a linearized vector without promoter sequence was prepared by reverse PCR amplification, using an entry clone A as a template. The promoter was PCR amplified from wild-type N2 genomic DNA, using primers containing about 20 bp sequences of the promoter and homologous sequences (15-20 bp) of the linearized vector. The linearized vector and amplified promoter fragment were recombined to generate entry clone A, using ClonExpress®II One Step Cloning Kit (Vazyme Biotech Co.).

Construction of an entry clone B containing a gene of interest

An entry clone B contributing sequences of slot 2 in the expression plasmid contains sequence of a target gene. A large part of entry clones B containing a gene of interest were constructed by BP recombination reactions using pDONR™ 221 donor vector (Invitrogen). The DNA sequences were amplified by PCR with the primers containing *att*B1 and *att*B2 recombination sites. A small part of entry clones B containing a gene (receptor used in this study) were constructed by the In-Fusion method.

Construction of an entry clone C

An entry clone C contributing sequences of slot 3 in the expression plasmids contains a sequence of *unc-54* 3' UTR, *sl2d::GFP*, or *sl2e::TagRFP-t*. The "C" entry clones were constructed by use of pDONR-P2R-P3 donor vector through standard BP reactions. The corresponding PCR products with *att*B2R and *att*B3 sites were amplified by PCR. The "C" entry clone containing *unc-54* 3' UTR, *sl2d*::*GFP*, or *sl2e*::*TagRFP*, were used to construct expression plasmids. All primers and related information for cloning these promoters and genes are listed in key resources table.

Behavioral assays

Mock and salt conditioning

All behavioral experiments were conducted using the synchronized day-1 adult worms. The chemotaxis to NaCl and salt chemotaxis learning of mock- and NaCl/food-deprivation association-conditioned (salt-conditioned, hereafter) animals were performed on test agar plates. For NaCl/food-deprivation association conditioning (salt conditioning), worms on culture plates were washed out with 100 mM NaCl-CTX solution (100 mM NaCl, 5 mM KH_2PO_4/K_2HPO_4 with pH 6.6, 1 mM $CaCl_2$, and 1 mM $MgSO_4$) and transferred into a 1.5 mL centrifugal tube. The worms were washed three times with about 1 mL 100 mM NaCl-CTX solution for about 5 min to remove bacteria from worm's body. Then, the worms were soaked in 1.2 mL 100 mM NaCl-CTX solution for about 14 min. Lastly, the worms were washed with CTX buffer without NaCl one time to remove NaCl. Total time for these manipulations was about 20 min.

For mock conditioning, the worms were treated with NaCl-free CTX buffer (5 mM KH_2PO_4/K_2HPO_4 with pH 6.6, 1 mM $CaCl_2$, and 1 mM $MgSO_4$) using the same procedure as that for the salt conditioning.

Assaying induction time course of SCL

The tested wild-type N2 animals were conditioned by the association of food-deprivation with the treatment of NaCl-free (for mock-conditioning) CTX solution and 100 mM NaCl-containing CTX solution (for salt-conditioning) with varied treatment duration (10 min, 20 min, 30 min, and 60 min), respectively.

Preparing test agar plates

A test of chemotaxis to NaCl or salt chemotaxis learning (SCL) was performed on a test NGM plate in a Petri dish of 9 cm diameter at room temperature of 20°C. The test plates contain two chemotaxis test regions without (region A) or with (region B) 20 mM NaCl in opposite direction. The plates were prepared with following protocol. 15 mL hot agar solution (5 mM KH_2PO_4/K_2HPO_4 with pH 6.6, 1 mM $CaCl_2$, 1 mM $MgSO_4$, and 2% agar) at about 80°C was poured into the Petri dish. After naturally cooled and solidified, two circular test regions in 3.5 cm diameter close to the edge of dish in the opposite direction were made. The agar in the test regions was cut with a 3.5 cm dish and then removed. The test regions were refilled with a hot agar solution with 20 mM NaCl (20 mM NaCl, 5 mM KH_2PO_4/K_2HPO_4 with pH 6.6, 1 mM $CaCl_2$, 1 mM $MgSO_4$, and 2% agar) or without NaCl (5 mM KH_2PO_4/K_2HPO_4 with pH 6.6, 1 mM $CaCl_2$, 1 mM $MgSO_4$, and 2% agar), respectively. The volume of refilling agar solution was carefully controlled to make sure that whole plate was even. Lastly, the test plates were incubated at 37°C for 3 hours and then were put on an even place at room temperature for 10 hours.

Chemotaxis and salt chemotaxis learning assay

The mock- or salt-conditioned animals of number about 200 in about 20 μL solution were transferred onto the center of a test plate. The residual solution was absorbed with tissue. Let worms freely move on the test plate for 10 minutes. Then, a circle of 0.5 mM sodium azide was immediately made around the edge of two test regions to paralyze worms. The number of worms in the test regions were counted under a stereomicroscope. The index of chemotaxis to NaCl in mock- or salt-conditioned animals was calculated as ($Number_B$ - $Number_A$) / ($Number_B$ + $Number_A$). Here, $Number_A$, the number of worms within the test region without NaCl; $Number_B$, the number of animals within the test region with 20 mM NaCl. The learning index was calculated as the average chemotaxis index of mock-conditioned animals minus the chemotaxis index of salt-conditioned worms. All conditioning and chemotaxis tests were performed at 20°C.

Assaying recovery time course of SCL memory-loss

The tested wild-type N2 animals were mock- and salt-conditioned for 20 min. Then, let animals freely move on the food-free test plate for different time (5 min, 10 min, 20 min, 30 min, 40 min, 50 min, and 60 min). After the given time, the animals' distribution on the plate was recorded by using a mobile phone.

Genetic and chemogenetic manipulations of tested neurons

Genetic manipulations of tested neurons

We employed neuron-specific extrachromosomal expression of TeTx to genetically block vesicle fusion with the plasma membrane and thus neurotransmitter release in the tested neurons. TeTx is a specific protease of synaptobrevin.[69] It is used successfully to inhibit the chemical neurotransmission in tested neurons in *C. elegans*.[71,72,76,95]

Chemogenetic manipulations of tested neurons

To tempo-spatially silence the tested neurons, we used chemogenetic neuronal manipulation. In short, we used neuron type-specific promoters to drive expression of a *Drosophila HisCl1* gene encoding histamine-gated chloride channel subunit[95] in the tested neurons and employed 10 mM histamine to activate the chloride ion channel.[71–73,76,95] To drive *TeTx* or *HisCl1* expression in ASER, RIC, and RIS, the promoters *gcy-5p* (3.2 kb, in ASER), *tbh-1p* (4.5 kb, in RIC), and *frpr-10p* (2 kb, in RIS) were used, respectively. HisCl1 channel may have a low probability of opening without ligand histamine, causing a leaking current in some cases. To reduce the leaky effect on tests, we injected the amount of the *HisCl1* plasmids by reducing its concentrations to 15 ng/uL.

For chemogenetic inhibition of the tested neurons in learning stage, we conditioned animals with 10 mM histamine in solutions used in mock- and salt-conditioning. Then, we tested the treated animals' chemotaxis on normal test plates.

For chemogenetic inhibition of the tested neurons in memory recalling stage, we used a test agar plate containing10 mM histamine to assay the normally conditioned animals' chemotaxis behavior. These test plates were prepared with the same procedures for preparation of the normal test plates, except all agar solutions contained10 mM histamine. To prepare the agar solutions containing 10 mM histamine, a stock solution of histamine (1 M in CTX buffer) was diluted with ultrapure water into a 100 mM working solution, and 10% (v/v) working solution was added into agar solutions at approximately 60°C before preparing the plates.

Pharmacological treatment of animals with tyramine and octopamine

Tyramine (TA) and octopamine (OA) are administered at both learning and memory recalling stages, to test their potential roles in the salt-chemotaxis learning. 10 μM TA or OA or both of them in solutions for mock- and salt-conditioning, or in agar solutions for preparing test plates, are used. Test plates containing TA and OA were prepared with the same procedures for preparation of the normal test plates, except agar solutions contained 10 μM tyramine, or octopamine, or both of them. To prepare these agar solutions, a stock solution of tyramine or octopamine (200 mM in CTX buffer) was diluted with ultrapure water into a 1 mM working solution, and 1% (v/v) working solution was added into agar solutions at approximately 60°C before preparing the plates.

Calcium imaging

The calcium (Ca^{2+}) responses in neuronal soma were measured by detecting changes in the fluorescence intensity of the genetically encoded Ca^{2+} indicator R-GECO1 and G-CaMP3.0. A home-made microfluidic device was used for calcium imaging, as previously described.[71–74,76] Briefly, a mock- or salt-conditioned worm was loaded into the worm channel of the microfluidic chip with its nose exposed to solutions under laminar flow. For each Ca^{2+} assay with duration of 80 s in ASER, RIS, RIC, and AIY, NaCl stimulation was performed by a switch between CTX buffer and 50 mM NaCl-CTX solution: CTX for 20 s—NaCl-CTX for 30 s—CTX for 30 s. The osmolarities of all solutions used for Ca^{2+} imaging were adjusted to 350 mOsmM with sucrose. The solutions were delivered via programmable automatic drug-feeding equipment (MPS-2, InBio Life Science Instrument Co. Ltd, Wuhan, Hubei Province, China). R-GECO1.0 was excited by 525–530 nm light emitted by an Osram Diamond Dragon LTW5AP light-emitting diode (LED) model (Osram, Marcel-Breuer-Strasse 6, Munich, Germany) mounted to a multi-LED light source (MLS102, InBio Life Science Instrument Co. Ltd) and filtered by a Semrock FF01-593/40-25 emission filter (IDEX Health & Science, LLC, Oak Harbor, WA, USA) under an Olympus IX-70 inverted microscope (Olympus) equipped with a 40× objective lens (numerical aperture (NA) = 1.3, Carl Zeiss MicroImaging GmbH, Göttingen, Germany). Fluorescence images were captured by an Andor iXonEM+ DU885K EMCCD camera (Andor Technology plc., Springvale Business Park, Belfast, UK) with 256 × 256 pixels at 10 frames per second. Each animal was exposed under fluorescent excitation light for 30 s before recording to reduce the light-evoked calcium transients and was recorded once only. The averaged fluorescence intensity in each frame of the region of interest (ROI) of the soma was captured and analyzed by using Image-Pro Plus 6 (Media Cybernetics, Inc., Rockville, MD, USA). The average signal of an adjacent ROI in all frames was used to subtract the background. The average fluorescence intensity within the initial 20 s before stimulation was taken as basal signal F_0. The changes in fluorescence intensity relative to the initial intensity F_0, $\Delta F = (F - F_0) / F_0$, were plotted as a function of time for all curves. The Ca^{2+} signals, ΔF, were displayed as the mean values in various colors and SEM in light grey using IGOR Pro 6.10 (WaveMetrics, Inc., Lake Oswego, OR, USA), as heatmap using Matlab-R2019a (MathWorks, Nidec, MA, USA), or boxplot using GraphPad Prism 8 (GraphPad Software, Inc., San Diego, CA, USA).

Confocal fluorescence imaging

All confocal fluorescence imaging was performed using an Andor Revolution XD laser confocal microscope system (Andor Technology plc., Springvale Business Park, Belfast, UK) based on a spinning-disk confocal scanning head CSU-X1 (Yokogawa Electric Corporation, Musashino-shi, Tokyo, Japan). The confocal system was mounted on an Olympus IX-71 inverted microscope (Olympus, Tokyo, Japan) and controlled by Andor IQ 1.91 software. Live young adult worms were mounted on a 2% (w/v) agarose pad with 10 mM levamisole (Sigma-Aldrich). All fluorescent images were imaged by ×60 objective lens (numerical aperture = 1.45, Olympus) and captured by an Andor iXonEM+ DU-897D EMCCD camera. The images were displayed using Image J 1.52o software (Wayne Rasband, National Institutes of Health, USA).

Locomotion analysis

Day-1 young adult worms cultured by standard methods were transferred onto an area in NGM plates (diameter 6 cm) with a thin layer of OP50 and allowed them to move freely for 3 min. Worm locomotion was recorded under a Zeiss Discovery V8 stereomicroscope (Carl Zeiss MicroImaging GmbH, Göttingen, Germany). The image sequences were captured with an Andor iXonEM+ DV885K EMCCD camera at 10 frame per second. The worm locomotion speed was analyzed by use of Worm Lab software.

Neuropeptide-receptor interaction prediction with Alphafold2

The receptor structure is first modeled independently using AlphaFold2 and then input into the protein template library. To model the interaction between the neuropeptide and the receptor, link the two sequences with 30 glycine, and use AlphaFold2 to predict the structure of the neuropeptide-receptor complex. Parameter settings: iteration numbers (3, 6, 9, 12, 15, 18, 20) and randomly set 10 seed numbers. Among the five models, as long as one generates a distance of less than 8 Å between any Cβ atoms of the neuropeptide and the receptor, and the binding site of the neuropeptide is located at the N-terminus of the receptor, it is considered valid. The hardware used includes 4 NVIDIA A40 GPUs, and the MSA search employs default parameters.[50]

FRPR-10 expression in *X. laevis* oocytes and whole-cell current recording

FRPR-10 expression in X. laevis *oocytes*

frpr-10 cDNAs were flanked with *BamH*I and *Hind*III sites by PCR and cloned into a pGH19 vector with by T4 ligase. The cRNAs of *frpr-10*, *GIRK1*, and *GIRK4*, were prepared using an mMachine™ T7 kit (Thermo Fisher scientific, Waltham, MA, USA). The sense of *frpr-10* (50 ng), GIRK1 (0.5 ng), and GIRK4 (0.5 ng), were injected into a *X. laevis* oocyte. The cRNA-injected oocytes were incubated at 18°C in ND96 medium (96 mM NaCl, 2.5 mM KCl, 1 mM $MgCl_2$ and 5 mM HEPES, pH 7.6) for 2-5 d before recording.

Whole-cell current recording

Whole-cell current was made using the two-electrode voltage-clamp technique at a holding potential of -80 mV as described.[67,68] The recording chamber was continuously perfused with ND96 medium. To assay activation of GIRK channels, we equilibrated oocytes in high K^+ medium (96 mM KCl and 2.5 mM NaCl instead of 2.5 mM KCl and 96 mM NaCl) to reverse the K^+ gradient and measured inward currents before, during and after addition of test peptide. Data were acquired with Clampex 8.0 software (Molecular

Devices, San Jose, CA, USA) and analyzed offline with Clampfit (Molecular Devices, San Jose, CA, USA). Peptides of 98% purity were synthesized by the Guoping Pharmaceutical Company (Hefei, Anhui Province, China).

QUANTIFICATION AND STATISTICAL ANALYSIS

Data of chemotaxis and the learning index are displayed as box plots, with each dot representing the data from each independent test. We performed experimental repetition for the tested animals of varied genotypes and WT N2 control on the same day. However, we performed more repetition for tested animals of some genotypes than that for the N2 control. Because the behavioral test results of N2 animal was rather repeatable or stable. We made effort to maintain consistent environmental conditions, such as temperature and humidity, and implemented randomization of the experimental order to minimize systematic bias. The Ca^{2+} signal data are expressed as heatmaps, box plots, or as the means ± SEM indicated by solid traces ± gray shading. Data were statistically analyzed using software packages in GraphPad Prism 9.5 (GraphPad Software, Inc., San Diego, CA, USA). When the comparison was limited to 2 groups, a two-tailed *t* test with unpaired samples was used to analyze differences and calculate *p*-values. When more than two groups of data were compared, data were analyzed by ordinary one-way or two-way analysis of variance (ANOVA), with recommended post hoc tests in the GraphPad Prism 9.5 software package. Dunnett's or Sidak's multiple comparison correction was applied when multiple samples were compared to a single sample, i.e., wild-type N2 or other controls. Tukey's multiple comparison correction was used when multiple samples were compared. The *p*-value is indicated as follows: ns, not significant, $^{*}p < 0.05$, $^{**}p < 0.01$, $^{***}p < 0.001$, $^{****}p < 0.0001$, and in different colors for varied comparison.